



# The Paton WELDING JOURNAL

Issue  
**07**  
2018

Published Monthly Since 2000

English translation of the monthly «Avtomaticheskaya Svarka» (Automatic Welding) journal published in Russian since 1948

## EDITORIAL BOARD

Editor-in-Chief

**B.E. Paton**

*Scientists of PWI, Kyiv*

**S.I. Kuchuk-Yatsenko** (*vice-chief ed.*),

**V.N. Lipodaev** (*vice-chief ed.*),

**Yu.S. Borisov, G.M. Grigorenko,**

**A.T. Zelnichenko, V.V. Knysh,**

**I.V. Krivtsun, Yu.N. Lankin,**

**L.M. Lobanov, V.D. Poznyakov,**

**I.A. Ryabtsev, K.A. Yushchenko**

*Scientists of Ukrainian Universities*

**V.V. Dmitrik**, NTU «KhPI», Kharkov

**V.V. Kvasnitsky**, NTUU «KPI», Kyiv

**E.P. Chvertko**, NTUU «KPI», Kyiv

*Foreign Scientists*

**N.P. Alyoshin**

N.E. Bauman MSTU, Moscow, Russia

**Guan Qiao**

Beijing Aeronautical Institute, China

**M. Zinigrad**

Ariel University, Israel

**V.I. Lysak**

Volgograd STU, Russia

**Ya. Pilarczyk**

Welding Institute, Gliwice, Poland

**U. Reisgen**

Welding and Joining Institute, Aachen, Germany

**G.A. Turichin**

St. Petersburg SPU, Russia

### Founders

E.O. Paton Electric Welding Institute, NASU

International Association «Welding»

### Publisher

International Association «Welding»

### Translators

A.A. Fomin, O.S. Kurochko, I.N. Kutianova

*Editor*

N.G. Khomenko

*Electron galley*

D.I. Sereda, T.Yu. Snegiryova

### Address

E.O. Paton Electric Welding Institute,

International Association «Welding»

11 Kazimir Malevich Str. (former Bozhenko Str.),

03150, Kyiv, Ukraine

Tel.: (38044) 200 60 16, 200 82 77

Fax: (38044) 200 82 77, 200 81 45

E-mail: journal@paton.kiev.ua

www.patonpublishinghouse.com

State Registration Certificate

KV 4790 of 09.01.2001

ISSN 0957-798X

DOI: <http://dx.doi.org/10.15407/tpwj>

### Subscriptions

\$348, 12 issues per year,

air postage and packaging included.

Back issues available.

All rights reserved.

This publication and each of the articles contained

herein are protected by copyright.

Permission to reproduce material contained in this journal must be obtained in writing from the Publisher.

## CONTENTS

### SCIENTIFIC AND TECHNICAL

*Smiyan O.D.* Gas emission and redistribution of hydrogen in aging of welded structures from different metallic materials ..... 2

*Akhonin S.V., Belous V.Yu., Selin R.V., Vrzhyzhevsky E.L. and Petrychenko I.K.* Electron beam welding and heat treatment of welded joints of high-strength pseudo- $\beta$  titanium alloy VT19 ..... 10

*Razmyshlyayev A.D., Vydmysh P.A. and Ageeva M.V.* On the problem of modeling transverse magnetic field structure in welding pool zone ..... 15

### INDUSTRIAL

*Kulik V.M.* Technical parameters and features of manufacturing high-pressure vessels for natural gas transportation ..... 20

*Petrushinets L.V., Falchenko Yu.V., Fedorchuk V.E. and Shinkarenko V.S.* Possibilities of manufacturing three-layer welded honeycomb panels from aluminium alloys ..... 25

*Matvienko V.N., Leshchinsky L.K. and Mazur V.A.* Calculation of penetration zone dimensions in surfacing of rolls for billet continuous casting machines ..... 30

*Kuskov Yu.M. and Soloviov V.G.* Experimental study of slag and metal pool rotation during the electroslag process in current-supplying mould ..... 33

### NEWS

International Conference «Titanium 2018. Production and Application in Ukraine» ..... 36

# GAS EMISSION AND REDISTRIBUTION OF HYDROGEN IN AGING OF WELDED STRUCTURES FROM DIFFERENT METALLIC MATERIALS

O.D. SMIYAN

E.O. Paton Electric Welding Institute of the NAS of Ukraine  
11 Kazimir Malevich Str., 03150, Kyiv, Ukraine. E-mail: [office@paton.kiev.ua](mailto:office@paton.kiev.ua)

The results of investigations of hydrogen behavior in process of aging of welded structures from different materials were analyzed. Gradation of the processes taking place in metal at aging was carried out and reasons of reduction of crack resistances in welded joints at room temperatures were found. The mechanism was proposed, which explains spontaneous hydrogen emission from metal in process of aging, reasons and consequences of these processes. 22 Ref., 2 Tables, 11 Figures.

**Keywords:** *aging of welded structures, hydrogen, crack resistance, boson, mechanism, cold crack*

Cold cracks are formed in welded joints of different class steels as a consequence of phase transformations resulting in decrease of metal strength properties (for example, formation of hardening structures), presence of diffusion-mobile hydrogen (DMH) and effect of welding stresses. Cold cracks are formed in cooling stage at temperatures below 423 K as well as in aging of welded structures at room temperature during some time after welding. Considerable number of works (for example [1–6]) are dedicated to problems related with investigation of the reasons and mechanisms of formation of cold cracks in welded joints of steels and titanium alloys of different composition and development of activities on their prevention.

Concept of aging can be found in technical literature. It is implied as isothermal holding of metal after the end of welding in process of welded joint cooling at some temperature (usually  $T = 373\text{--}423$  K in a period from 0 min to 8 h) for partial release of welding stresses and removal of excessive DMH. Such an operation results virtually in complete recovery of plastic properties of metal and, therefore, further aging of this welded joint at room temperature does not already lead to formation of cold cracks in it. Thus, this topic was investigated for different steels starting from the middle of XX century (for example, it is reflected in works [7–9]). This paper does not cover these problems. Aim of the present paper is an analysis of the processes taking place in metal of welded joints and structures during aging only at room and climatic temperatures (therefore aging is not discussed here), which are used in real operation of many steel parts and structures susceptible to formation of cold cracks

under these conditions. This problem is bought up comparatively rare and it is not studied enough.

It is known that performance of some technological operations (fusion welding, rolling, heat treatment) of different steels and alloys provokes spontaneous emission at room temperatures during some time of so-called diffusion-mobile hydrogen. Its amount and distribution in the welded joint can be controlled by various methods of analysis. The most widespread of them is a glycerol method, when the welded sample is immersed into a bath with glycerol and the places and frequency of hydrogen bubbles emission on its surface is controlled [8]. It is supposed that content of remaining in metal hydrogen (so-called residual hydrogen — RH) stays constant at room temperature during long time. It is determined that DMH emission mainly takes place on fusion line, HAZ-BM boundary and grain boundaries. For high-strength steels, mainly of martensite and martensite-bainite classes, this phenomenon is related with appearance of cold cracks in the welded joints in process of their cooling to temperatures below 373 K and further aging at room temperatures (Figure 1). It is widely stated that in 3–10 days of aging amount of emitted DMH reduces to safe level and cracks are not formed in future.

It is assumed that no phase transformations take place in process of aging, only diffusion (spontaneous release of hydrogen from metal) and relaxation processes causing transfer of plastic deformations from grain boundaries to grain body [7] are observed. This results in rise of ductility and cold crack resistance. Simultaneously, there is reduction of electrical resistance of steel that indicates ordering of metal atomic structure [9].

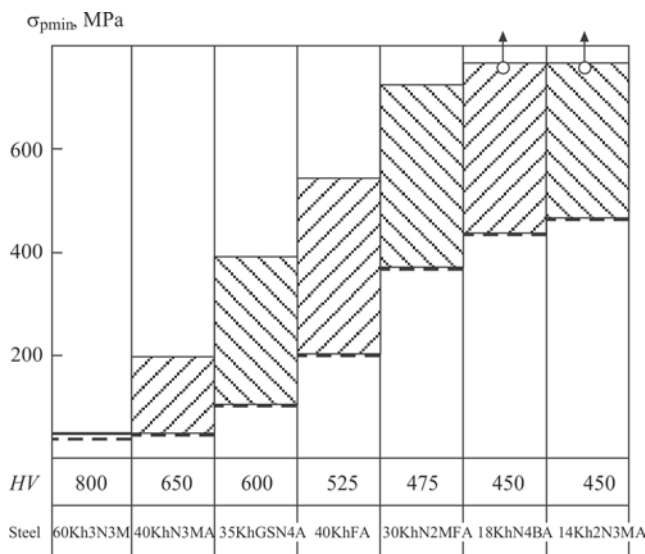


**Figure 1.** Effect of DMH content (boson  $H^-$ ) in deposited metal on cold crack resistance of different steels. T-sample LTPP2-3, electrodes UONI 13/45 (dashed line —  $[H^-] = 4$  ppm; solid line —  $[H^-] = 1$  ppm (2)) [1]

Numerous empirical observations were analyzed and on their basis technological solutions were proposed. They allow eliminating appearance of cold cracks during aging of the welded joints from low-alloy high-strength steels [5, 6, 10]. However, deep systematic investigations of the processes taking place in metal of welded joint during its aging have not been carried out, the reason and mechanism of negative effect of hydrogen on cold crack formation during aging are not determined. This has become a subject of investigation in this work.

The investigations, related with metal aging after technological treatment, are usually carried out on small-size samples, i.e. the process is virtually modeled. Under real conditions after welding is finished many products are used at room and climatic temperatures for a long time (years) in media containing hydrogen in different forms, i.e. in form of moisture in air, condensate (mist), running water (rain), vapors of acids in atmosphere, working hydrogen-containing fluids etc., however, for such conditions an effect of «external» hydrogen of the medium, from which it is absorbed by metal before as well as in process of operation, is not considered.

Investigations carried by us together with I.K. Pokhodnya and colleagues [11] showed that DMH is a negative quasi-ion of hydrogen  $H^-$ . Next works [12] demonstrated that hydrogen absorbed by metal is contained in solid body simultaneously in two states, i.e. in form of  $H^-$  and  $H^+$  quasi-ions.  $H^-$  quasi-ion has quantum properties of boson, namely ultramobility in solid body. A mass transfer coefficient of hydrogen-boson (diffusion coefficient in specific case) is more than hydrogen diffusion coefficient (fermion) in

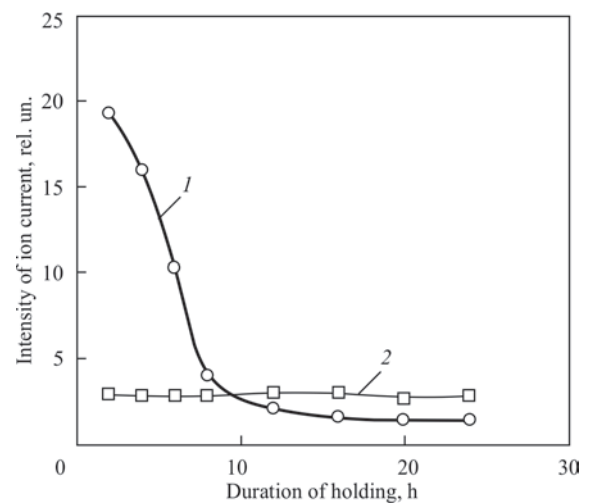


**Figure 2.** Dependence of intensity of secondary ions of hydrogen  $H^-$  (1) and  $H^+$  (2) on duration of exposure in ultrahigh vacuum of preliminary hydrogen-charged samples of steel St3 [11, 12]

the same steel by several orders. For example, for steel 14Kh2GMR at room temperatures in 40 h after welding it reaches  $D^{H^-} = 1.95 \cdot 10^{-3} \text{ cm}^2/\text{s}$  value and after aging during one month  $5.85 \cdot 10^{-7} \text{ cm}^2/\text{s}$ . This explains spontaneity of DMH emission under these conditions.  $H^+$  hydrogen quasi-ion has the fermion properties (this is so-called residual or proton-ionized hydrogen), which is removed from metal only in process of heating or melting.

It is determined [12] that under certain conditions (temperature, metal composition) hydrogen-boson can transform into another form, namely hydrogen-fermion and vice versa. For structural steels such a critical temperature is 602 K.

It is found that content of DMH is higher in subsurface weld metal layers (Figure 3). Relationship between  $H^-$  and  $H^+$  changes from the surface to weld metal depth (Figure 4) and also in variation of met-

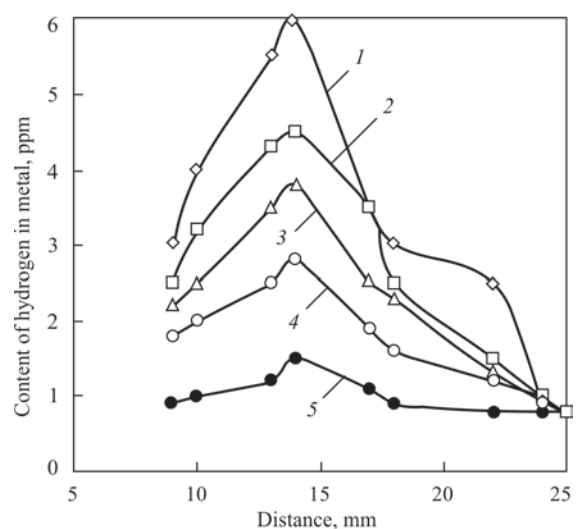


**Figure 3.** Change of hydrogen distribution in St3 steel sample in aging after welding in 1, 2, 3, 4 and 5 h, respectively (on x-coordinate — distance from weld metal surface [14])

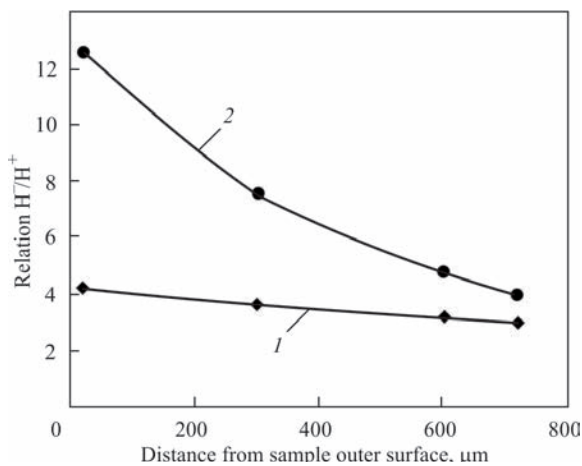


**Figure 4.** Change of H-/H+ relationship on normal section radius of cylinder sample from steel 20 along atomically pure fracture surface after heat treatment (1 — normalizing; 2 — quenching) [12]

al composition in process of aging as well as during operation. For example, introduction of a nickel in deposit metal results in change of H-/H+ relationship at preservation of total content of hydrogen (boson and fermion) (Table 1). Hydrogen-boson is one of the main reason of cold cracks initiation [12].

Analysis of the results of aging process observation and experimental data on control of DMH and RH content in metal of welded joints, carried earlier by different authors, showed that all cases of aging of steels and alloys, being accompanied by spontaneous emission or redistribution of hydrogen at room temperatures can be classified on various groups that differ by nature, dynamics of process or level of hydrogen effect on metal mechanical properties:

1. In process of aging independent on its duration the structure and phase composition of metal are preserved and the changes of composition (including on hydrogen) do not reach critical values. Metal structure is energy stable. Probability of cold cracks appearance is low or completely absent.

2. In long-term aging metal of welded joint is subjected to changes of structure caused by stress relaxation and redistribution of chemical elements in the range of grains and their boundaries. Structures, formed in the welded joint, are energy non-equilibrium, unstable in time, their gradual stabilizing takes place in process of aging. There is a probability of appearance of cold cracks, in particular, in the first hours after welding.

3. In the process of long-term aging (or operation) there are phase transformations taking place in the metal, which promote changes of content of separate sections of metal of welded joint and solubility of hydrogen in them. The structures with large energy instability (hardening structures, martensite, bainite) and high welding stresses, zones with local plastic deformation, hydrogen solubility and increased local chemical inhomogeneity appear. Localizing of increased hydrogen concentration and intensity of its peaks reach and exceed the critical level for this steel, alloy. There are possible chemical reactions inside metal with formation of film iron hydrates, titanium hydrates or molecular gases (for example, hydrocarbons CH<sub>2</sub>, CH<sub>4</sub> type in high-carbon steels). Probability of cold crack appearance is very high.

4. Process of long-term aging (and operation) provokes change of charge state of hydrogen dissolved in metal and relationship between quasi-ions of hydrogen of different charge type. Probability of appearance of cold cracks depends on value of this relationship, coefficient of chemical inhomogeneity, intensity and locality of hydrogen concentration peak, possibility of chemical reaction between quasi-ions of hydrogen and steel components. Probability of cold cracks appearance is very high.

5. Duration of welded joint aging affects the intensity and parameters of final treatment of the products and their crack resistance. Formation titanium hy-

**Table 1.** Effect of composition of coating sprayed over on wire 09G2S on content of diffusion-mobile hydrogen (DMH) and residual hydrogen (RH) in deposit metal of steel 14Kh2GMR and on H-/H+ relationship [13]

No.	Wire coating composition	Content of hydrogen in deposit metal, 10 <sup>-4</sup> %				DMH relationship (H-) to RH (H+), H-/H+
		Separate determination		Total content		
		DMH, CA method	RH, LMA	Sum, DMH + RH	Determination by VM method	
1	Initial (base) metal	5.5	3.1	8.6	8	1.77
2	BM + 1.5 % N1	4.85	5.2	9.05	9	0.74
3	BM + 1.6 % Ni + 0.44 % REM, including 0.017 % Ce	1.9	7.2	9.1	8.5	0.26
4	BM + 0.45 % Y + 1.8 % Ni	4.6	4.2	8.8	9.5	1.09
5	BM + 2 % Ni + 0.6 % REM, including 0.26 % Ce	2.3	6.6	8.9	8.9	0.35
6	BM + 0.3 % Y	5.2	3.9	9.1	10	1.33

*Designations:* BM — base metal; CA — chromatographic analysis; LMS — local mass-spectrum analysis; VM — vacuum melting method; REM — rare-earth metals (mixture).

drates and (or) film iron hydrates on grain boundary is possible. There is probability of cold crack formation.

Let us consider several examples illustrating proposed gradation of aging processes for different metals and alloys after their thermal or deformation treatment in different hydrogen-containing media.

Single-phase metals (for example, copper) as well as structural steels in a layer adjacent to fusion surface do not change their structure in process of aging. These materials can be used as model ones in analysis of welded joints of steels and titanium alloys. They allow evaluating and comparing the parameters and dynamics of hydrogen absorption by metal in process of local deformation, appearing in weld HAZ metal in its cooling as a result of effect of welding stresses and desorption of hydrogen in partial relaxation of welding stresses during aging.

There is a significant effect of medium, in which researched processes take place, on these processes (in welding — humidity of welding consumables; in deformation, aging and operation of welded products — content of hydrogen-containing medium and value of oscillations of climatic temperatures).

Figures 5 and 6, *a* show the data on change of a value and rate of hydrogen absorption by copper in process of its plastic deformation in different media, and Figure 6, *b* represents a rate of hydrogen desorption from the same samples of copper for 42 months of aging at room temperature. Copper is a single-phase and ductile metal, therefore, phase and structural changes had no effect on the studied processes and

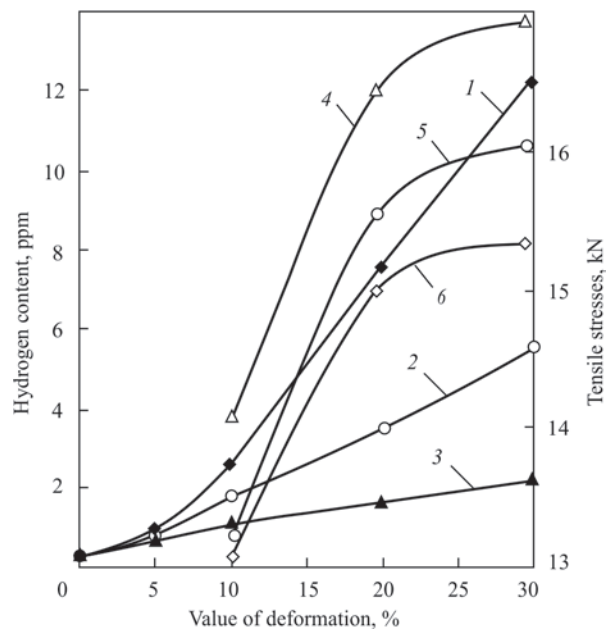


**Figure 5.** Dependence of hydrogen content in copper (curves 1–3) and value of loading (curves 4–6) on level of deformation in hydrogen gas (1), condensed (2) and running water media [16]

internal stresses caused by deformation and hydrogen dissolution are reduced to a minimum. Hydrogen absorption from hydrogen-containing medium by deforming metal at room temperatures is provoked by influence of structure-deformation effect described in work [15], desorption of hydrogen is relaxation of stresses in long-term aging.

Content and distribution of hydrogen in the welded joint is significantly effected by content of this admixture in the medium, in which welding is carried

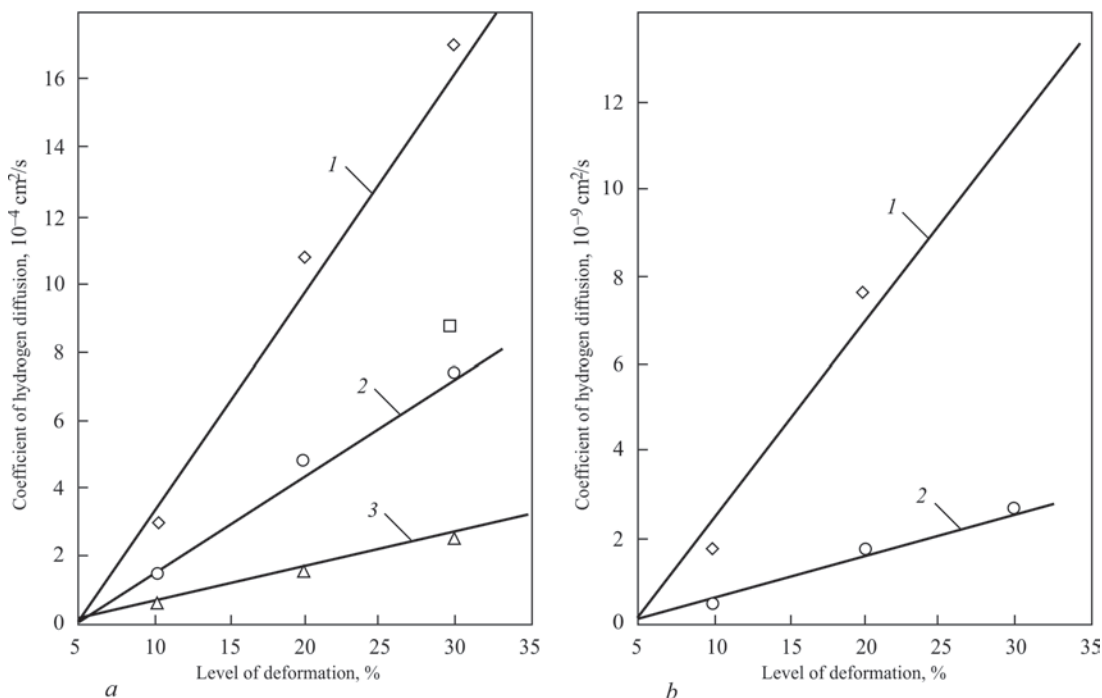


**Figure 6.** Change of hydrogen diffusion coefficient at its absorption by copper in (*a*) process of deformation (30 min) in hydrogen gas medium (1), (structured) water condensate (2), simple (running) water (3) and desorption (*b*) from the same copper samples after tension and aging during 42 months (1308 days) [15–17]

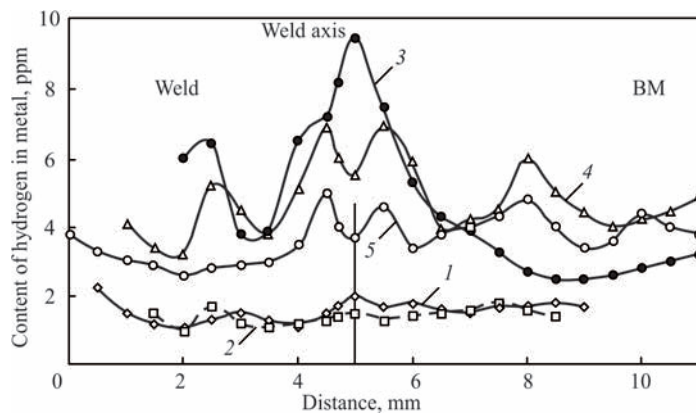


**Figure 7.** Distribution of hydrogen-boson in welded joint of steel 14Kh2GMR at different humidity of flux AN-17M: 1, 2 — humidity 0.017 %; 3, 5 — humidity 0.04 %. Aging after welding: 1 — 4 h; 2 — 5.5; 3 — 3; 4 — 4; 5 — 5. Local analysis of hydrogen content by LMA with TEE method [10]

out, and aging process. For example, change of flux humidity (as medium) in 14Kh2GMR steel welding results in increase of hydrogen content in metal (Figure 7) and to more inhomogeneous distribution of this admixture. This increases probability of crack appearance during the first hours of aging [10]. Decrease of flux humidity from 0.04 to 0.017 % is enough to make hydrogen distribution in the welded joint virtually homogeneous in 4 hours of aging and have minimal probability of crack appearance. It is typical that hydrogen removal from welded joint metal during aging is not identical in its different areas. The highest metal degassing rate is reached along the fusion surface (Table 2, Figures 8, 9) where structural changes in the process of aging have not been observed.

Investigation of process of hydrogen emission from this metal area by method of local mass-spectrum analysis with thermal electron extraction by electron-beam probe (LMA with TEE) [17] showed that hydrogen in process of aging is not desorbed from metal by continuous flow, but by the portions, pulses and curve of change of local content of hydrogen along fusion line during one month after welding

represents itself damping wave (Figure 9). The averaged values of experimental measurements match with distributions calculated on Fick's formula. A measurement error made  $10^{-4}$  ppm [17] that is considerably less than amplitude of concentration oscillations of hydrogen in the same area of the sample making several ppm units (Figure 9). Therefore, observed deviations from the curve, plotted by Fick's equation (dashed line on Figure 9) are not the measurement errors and reflect a real process of degassing of hydrogen from metal taking place in zone of surface fusion. Work [19] informs about pulsed nature of hydrogen emission from steel 9GS after rolling in the process of aging during cooling and room temperatures.

A wave nature of change of hydrogen content in process of long-term aging (during 10 months) was observed after multilayer argonarc welding of high-strength steel VNS-2. The parts from this steel produced by welding failed after 5–6 months in process of their operation as well as in conservation storage, i.e. without service loads. In order to find out the reasons of such behavior of material the welding coupons were made. They were used to cut out every month a strip of metal and produce the samples for the next investigation using LMA with TEE method on 0B768M unit at E.O. Paton Electric Welding Institute of the NAS of Ukraine. A discrete-spot analysis on local content of hydrogen by 5 parallel routes passing through weld and HAZ of the welded joint was carried out on each such sample. Obtained measurement results were averaged by the samples and

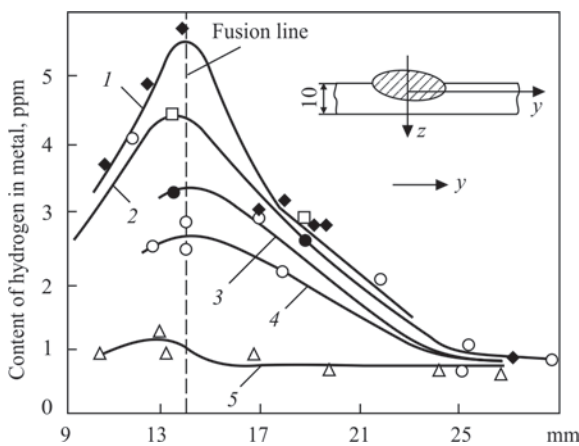


**Figure 8.** Distribution of hydrogen-boson in weld of St3sp (killed) steel in Y axis direction: 1 — directly after welding; 2 — in 1; 3 — 2; 4 — 24; 5 — 72 h after welding [20]

**Table 2.** Hydrogen diffusion in different areas of weld [18]

Steel, area	T, K	$D^H$ , $cm^2/s$	Type of structure
14Kh2GMR, weld	293	$6.8 \cdot 10^{-5}$	Martensite-bainite
14Kh2GMR, HAZ	293	$3.6 \cdot 10^{-7}$	Same
14Kh2GMR, fusion surface	293	$1.8 \cdot 10^{-4}$	»

at the end of year by the whole series of monthly measurements. Figure 10 shows the final results of these measurements. It is determined that in process of aging the total content of hydrogen in metal for 10 months of observations has changed insignificantly (curve 1 on Figure 10), but in separate areas of the welded joints the local concentration of hydrogen has increased from 5 ppm in metal (at once after welding) to 34 ppm in 7 months of aging of the welded coupons at room temperature. This is significantly higher than the critical limit of allowable hydrogen concentration in this steel (10 ppm) and caused product failure. Periodic variation of hydrogen content in the separate areas of welded joint was found in process of long-term storage, however, a curve reflecting these changes appeared to be rising. Metallographic examination of metal structure before and after aging showed incomplete martensite transformation in metal with formation of carbide grid, having lower strength than metal and higher hydrogen solubility. It is determined that there are migration and redistribution of hydrogen-boson in this martensite steel in the field of local internal stresses and microareas of plastic deformation at room temperature during aging. Hydrogen-boson is concentrated along the grain boundaries and in the zones of their joining where dilatons and clusters of vacancies are formed. Hydrogen mobilizes in them developing significant inner pressure. This promotes partial decay of martensite with carbide grid precipitation. Hydrogen from the surrounding metal migrates in these areas since its solubility in carbide is considerably higher than in metal. As a result process of metal degradation is accelerated. The analysis registers a rise of local concentration of hydrogen in the separate areas at preservation of its average content in metal (curve 3, Figure 10). Hydrogen-boson reacts with carbon forming with it hydrocarbons, for the first  $\text{CH}_2$ , then  $\text{CH}_4$ . These processes (increase of hydrogen concentration in carbide grid, formation of new portions of dilatons, growth of inner pressure, formation of new portions of hydrocarbons) take place simultaneously, i.e. this is synergetic process. It can be assumed that in a period of formation of new portions of hydrocarbons there is increased consumption of hydrogen and concentration curve will show decrease of its local concentration and inner pressure, process of formation of new portions of hydrocarbons fails. Local concentration of hydrogen in a carbide grid rises again to the critical level when process of formation of hydrocarbons is reactivated and defect zones increase. There is appearance of microcracks in the carbide grid which grow in process of aging. At seven months of aging the crack in metal rises to the critical values. Local concentration of

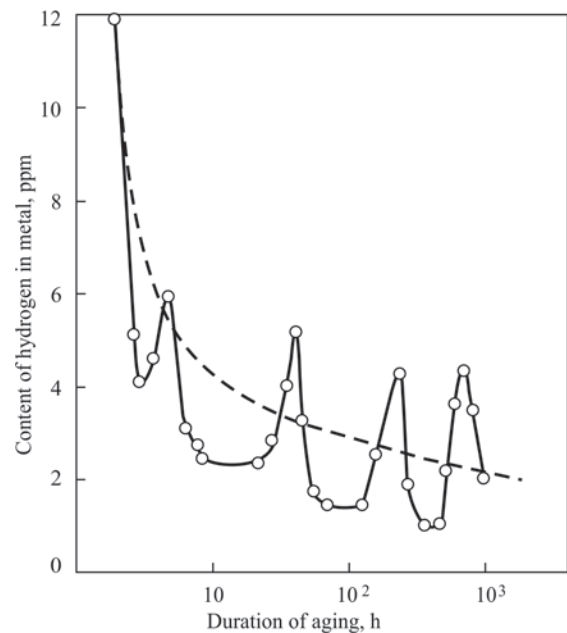


**Figure 9.** Change of hydrogen-boson concentration in weld-base metal fusion zone in process of aging of 14KhGMR steel samples at room temperatures. LMA with TEE method measurement of hydrogen by focused beam of electrons. Electric arc welding by ANP-1 electrodes (dashed line — change of hydrogen concentration in time on Fick's formula) [17]

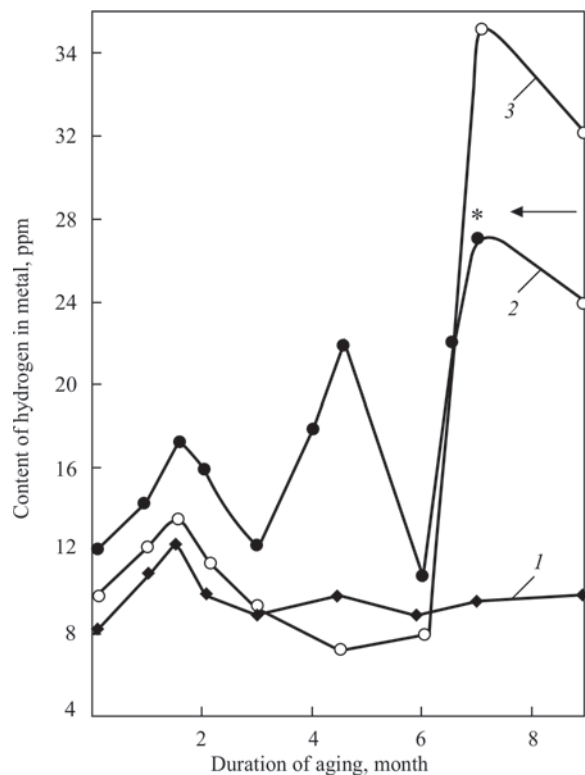


**Figure 10.** Change of hydrogen concentration at  $T = 300$  K in weld of steel VNS-2 during 9 months after welding; content of hydrogen in weld metal: average (1); in light/ferrite/ (2) and dark/carbide/ (3) strip (on diagram marked \* (indicated by arrow) — result of determination of hydrogen amount by vacuum-melting method in the sample cut from fracture zone)

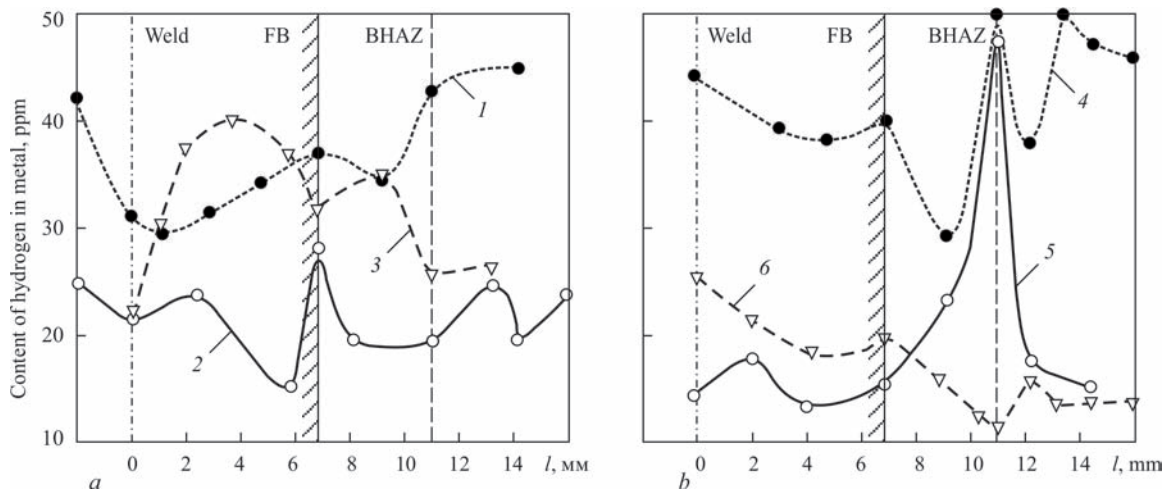


**Figure 11.** Hydrogen in welded joint of AT-3 alloy: without heat treatment (1, 4) and after annealing at  $T = 823$  K (2, 5) and 923 K (3, 6); in 3 h (a) and in 40 months (b) after welding:  $l$  — distance from weld axis; FB — fusion boundary; BHAZ — boundary of HAZ [21]

hydrogen in carbide grid reaches 32–34 ppm (curve 1 on Figure 10). Plastic deformation is activated in ferrite. During it the dislocation cores capture hydrogen from the medium [15] and there is also intensive increase of local hydrogen concentration in it. Ferrite with such high local content of hydrogen (28.0 ppm) (curve 2 on Figure 10) is also susceptible to hydrogen embrittlement [17]. Thus, favorable conditions for metal degradation are developed in the localized zone of welded joint of steel VNS-2 in 7 months after welding in process of aging independent on effect of external (operation) loads, which only insignificantly (less than for 1 month) accelerate failure process.

One more interesting materials science aspect of the consequences of long-term aging is a change of final technological operations, in particular, mode and nature of welded joint annealing performed before and after long-term aging (Figure 11). It is determined that if argonarc welded product of alloys AT-3 is used in structure at once after welding or during a month after, it is reasonable to use incomplete annealing ( $T = 823$  K) and this is enough for removal of welding stresses and obtaining optimum mechanical characteristics of AT-3 alloy welded joint. There are no dangerous situations related with significant local hydrogen saturation of local areas of welded joint (Figure 11, a) in such metal. Moreover, complete annealing ( $T = 923$  K) results in somewhat increase of hydrogen content in weld metal and HAZ (curve 3 on Figure 11, a). However, if welded product ages during three or more years and only after it is used in the structure than there is a need in carrying out complete annealing ( $T = 923$  K) since long-term aging provokes in welded joint metal some structural changes. They are accompanied by redistribution of some chemical elements, in particular, hydrogen, namely its content on HAZ–BM boundary rises and after incomplete

annealing the local concentration of hydrogen in this area reaches critical values up to 51 ppm (curve 5 on Figure 11, b). Work [22] informs that the welded joints of titanium-based alloys contain a narrow resolidification zone with high internal stresses on HAZ–BM boundary. The structural components of this band (plate) in process of aging are «covered» with film carbides, oxides, titanium hydrates. As a result in this area of metal the stresses rise, and strength drops.

Hydrogen segregation coefficient in these areas reaches 3.0–3.5 values [22]. In our case (Figure 11, b, curve 5) this coefficient is still higher and equals 8, moreover, the concentration peak is acute, i.e. this area of metal has high probability of crack formation. The nature of hydrogen distribution curves on welded joint section in three years of aging (Figure 11, b, curves 5 and 6) indicate that the high internal stresses appearing in this area of metal are not entirely eliminated, but can be removed at complete annealing (curve 6 on Figure 11, b). This fact shall be taken into account during manufacture of welded products and structures.

## Conclusions

The mechanism was proposed, which explains the process of spontaneous gas emission of hydrogen in the process of aging at room temperatures, redistribution of this admixture in the products volume and change of tendency of welded joint metal to crack formation.

It is determined that aging at room temperatures results not only in loss by metal of part of earlier absorbed hydrogen as a consequence of relaxation of welding stresses in the welded joint, but redistribution of hydrogen inside metal if there are processes of phase (as in steel VNS-2) or structural as in alloy AT-3) transformations related with different solubili-

ty of hydrogen in separate phases or structures. This leads to increase of chemical inhomogeneity, appearance of the areas with local hydrogen concentration exceeding the critical values for this steel or alloy and provoking cold crack formation.

1. Makarov, E.L. (1981) *Cold cracks in welding of alloy steels*. Moscow, Mashinostroenie [in Russian].
2. Lobanov, L.M., Poznyakov, V.D., Makhnenko, O.V. (2013) Formation of cold cracks in welded joints from high-strength steels with 350-850 MPa yield strength. *The Paton Welding J.*, **7**, 7–12.
3. Kasatkin, B.S., Strizhius, G.N., Brednev, V.M. et al. (1993) Hydrogen brittleness and formation of cold cracks in welding of 25Kh2NMFA steel. *Avtomatich. Svarka*, **8**, 3–10 [in Russian].
4. Cwiek, J. (2007) Hydrogen degradation of high strength weldable steels. *J. of Achievements in Materials and Manufacturing Engineering*, **20**, 223–226.
5. Musiyachenko, V.F. (1983) *Weldability and technology of welding of high-strength steels*. Kiev, Naukova Dumka [in Russian].
6. Musiyachenko, V.F., Mikhoduj, L.I. (1990) Hydrogen in welding of high-strength steel and its influence on resistance of welded joints to cold crack formation. Kiev, Naukova Dumka, 161–168 [in Russian].
7. Akulov, A.I., Belchuk, G.A., Demyantsevich, V.P. (1977) *Technology and equipment of fusion welding*. Moscow, Mashinostroenie [in Russian].
8. Petrov, G.L., Million, A. (1964) Processes of hydrogen distribution in welded joints of carbon- and low-alloy steels. *Svaroch. Proizvodstvo*, **10**, 9–11 [in Russian].
9. Houdremont, E. (1959) *Special steels*. Moscow, Gostekhizdat [in Russian].
10. Smiyan, O.D., Kasatkin, B.S., Musiyachenko, V.F. et al. (1974) Influence of flux humidity on hydrogen distribution in welded joint of 14Kh2GMR steel. *Avtomatich. Svarka*, **5**, 72–77 [in Russian].
11. Pokhodnya, I.K., Shvachko, V.I., Smiyan, O.D. et al. (1988) Examination of diffusion-mobile hydrogen in low-alloy steels by method of secondary ion mass-spectrometry. In: *Proc. of 5<sup>th</sup> All-Union Conf. on Methods of Determination and Study of Gases in Metals Moscow*. Izd. A.A. Vernadskogo, GEOKhI, 145–148 [in Russian].
12. Smiyan, O.D. (2004) Hydrogen in metal as an ozone-free liquid. *Fizyka i Khimiya Tverdogo Tila*, **4**, 571–578 [in Ukrainian].
13. Musiyachenko, V.F., Melnik, I.S., Smiyan, O.D. et al. (1988) Hydrogen in high-strength weld metal microalloyed with rare-earth metals. In: *Information documents of CMEA*, **1**, 13–18 [in Russian].
14. Makara, A.M., Lakomsky, V.I., Grigorenko, G.M. (1968) Hydrogen distribution in welded joints during ageing. *Avtomatich. Svarka*, **2**, 1–5 [in Russian].
15. Smiyan, O.D. (2002) Atomic mechanism of interaction between medium substance and metal being deformed. *Fizyka i Khimiya Tverdogo Tila*, **4**, 662–667 [in Russian].
16. Bosak, L.K., Butkova, E.I., Smiyan, O.D. (1988) Examination of peculiarities of hydrogen sorption by solid metal with regard to HAZ in welding of copper. *Avtomatich. Svarka*, **8**, 36–38 [in Russian].
17. Vajnman, A.B., Melekhov, R.K., Smiyan, O.D. (1990) *Hydrogen embrittlement of components of high pressure boilers*. Kiev, Naukova Dumka [in Russian].
18. Smiyan, O.D., Kadyreva, K.K. (1976) New methods of direct experimental determination of diffusion coefficients of gas-forming impurities in metals of welded joints. In: *Diffusion processes in welding: Transact. Kiev, Znanie*, 20–21 [in Russian].
19. Tupilko, V.M., Zaika, V.I., Koval, G.M. et al. (1977) Pulsed nature of hydrogen emission from finished steel at room temperature. *Fiz.-Khim. Mekhanika Materialov*, **13**(1), 25–27 [in Russian].
20. Asnis, A.E., Ivashchenko, G.A. (1978) *Increase in strength of welded structures*. Kiev, Naukova Dumka [in Russian].
21. Blashchuk, V.E., Butkova, E.I., Smiyan, O.D. et al. (1990) Effect of annealing on nature of hydrogen distribution in welded joints of AT-3 alloy. *Avtomatich. Svarka*, **11**, 33–36 [in Russian].
22. Zadery, B.A., Shevchuk, T.V., Smiyan, O.D. et al. (1987) Peculiarities of transition area between HAZ and base metal in titanium alloy welded joints. *Ibid.*, **3**, 8–11 [in Russian].

Received 07.06.2018

# ELECTRON BEAM WELDING AND HEAT TREATMENT OF WELDED JOINTS OF HIGH-STRENGTH PSEUDO- $\beta$ TITANIUM ALLOY VT19

S.V. AKHONIN, V.Yu. BELOUS, R.V. SELIN, E.L. VRZHYZHEVSKY and I.K. PETRYCHENKO

E.O. Paton Electric Welding Institute of the NAS of Ukraine  
11 Kazimir Malevich Str., 03150, Kyiv, Ukraine. E-mail: [office@paton.kiev.ua](mailto:office@paton.kiev.ua)

Titanium pseudo- $\beta$  titanium alloys have high strength reaching 1200-1400 MPa in aged state, as well as high adaptability to manufacture in comparison with alloys of pseudo- $\alpha$ - or ( $\alpha + \beta$ )-structure. Such advantages of pseudo- $\beta$  titanium alloys, typical representative of which is high alloy VT19, make this class of titanium alloys promising for application in new technologies and equipment and during modernization of existing ones. The paper has studied the effect of mode of electron beam welding, modes of preheating and local heat treatment, as well as furnace annealing on properties of welded joints of pseudo- $\beta$  titanium alloy VT19 produced by electron beam welding. Variation of speed of electron beam welding of alloy VT19 does not allow changing within the significant limits the relation between  $\alpha$ - and  $\beta$ -phases in weld metal and heat-affected zone. Electron beam welding in combination with preheating allows regulating the relation between  $\alpha$ - and  $\beta$ -phases in welded joint metal and reducing the content of  $\beta$ -phase in weld metal of alloy VT19 from 91 to 53 % , as well as increasing the strength of welded joints from 876 to 937 MPa. 11 Ref., 2 Tables, 6 Figures.

**Keywords:** titanium, titanium alloys, pseudo- $\beta$  titanium alloys, electron beam welding, structure, properties, local heat treatment, annealing, strength

The main advantages of modern pseudo- $\beta$  titanium alloys are their high adaptability to manufacture in comparison with alloys with pseudo- $\alpha$ - or ( $\alpha + \beta$ )-structure, as well as their high strength properties. Such advantages of pseudo- $\beta$ -titanium alloys, the characteristic representative of which is the high alloy VT19 make this class of titanium alloys challenging

for using in new technologies and equipment, as well as in updating the existing ones [1]. The pseudo- $\beta$  titanium alloy VST5553 (Ti-5Al-5Mo-5V-3Cr) is already applied in aircrafts of Boeing production [2]. An important task is the development of welding technology and heat treatment modes of produced joints, which should provide the optimum phase composition and strength level of at least 0.90-0.95 of the base material strength. This requires the use of additional technological operations such as preheating and postweld heat treatment [3]. The electron beam welding (EBW) allows combining such technological operations as welding and heat treatment, which will provide the high quality of the produced joints [4, 5].

The aim of the work was to determine the influence of the EBW mode, the preheating and local heat treatment modes, as well as the modes of furnace annealing on the properties of pseudo- $\beta$  titanium alloy VT19 joints, made by EBW.

The specimens with dimensions of 200×100×8 mm were welded. The EBW was carried out in the updated installation UL-144 equipped with the power unit ELA 60/60. The preheating was carried out to the temperature of 400 °C, the temperature control was performed using thermocouples attached from the root side of the weld. The detailed procedure of preheating is described in work [6]. The scheme of preheating and local heat treatment (LHT) is shown

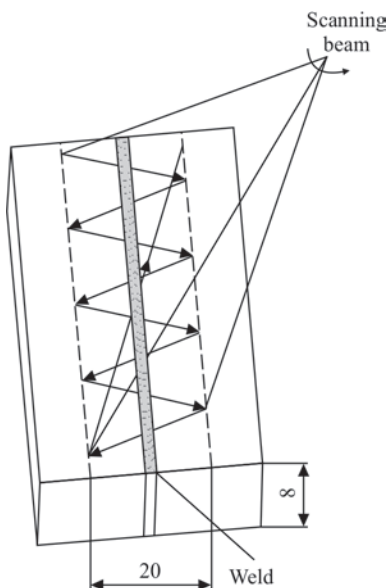


**Figure 1.** Scheme of scanning welded joint of the pseudo- $\beta$  titanium alloy VT19 at a local electron beam heat treatment (750 °C, 10 min)

in Figure 1. The treatment zone width was 20 mm. The electron beam power during the process of LHT was about 3 kW, and was subjected to correction for maintaining the temperature in the treatment zone at the level of 750 °C.

The welding was carried out at the following conditions:  $U_{acc} = 60$  kV,  $I_{beam} = 120$  mA. The joints were produced at two welding speeds of 7 and 11 mm/s.

Some of welded joints were subjected to preheating to the temperature of 400 °C before welding. The welded joints, produced with preheating after welding, were subjected to LHT in a vacuum chamber by the mode providing heating to the temperature of 750 °C and 10 min holding. A part of the joints after welding was subjected to furnace annealing, providing heating to the temperature of 750 °C, and holding for 1 h and the subsequent furnace cooling. The appearance of specimens of welded joints is shown in Figure 2. According to data of X-ray inspection and analysis of structure, in all the specimens, welded by EBW, such defects as pores, lacks of penetration, cracks, nonmetallic inclusions are absent.

The examinations of structure were carried out with the help of the optical microscope «Neophot-30», equipped with attachment for digital photography. The determination of the amount of  $\beta$ -phase in the weld metal, HAZ and base metal was performed experimentally on microsections. For this purpose, on scanned microsections the ratio of light regions of the structure, corresponding to  $\beta$ -phase, and dark regions of the structure, corresponding to  $\alpha$ -phase was evaluated.

The mechanical properties of base metal and produced welded joints are shown in Table 1.

The base metal of VT19 alloy contains equiaxial polyhedral grains with dispersed precipitations of  $\alpha$ -phase, uniformly distributed along the grain body (Figure 3, *a*). The size of  $\alpha$ -particles is 1–2  $\mu\text{m}$  and smaller. The amount of  $\beta$ -phase in the base metal in the as-rolled state is 44 % (Table 2).

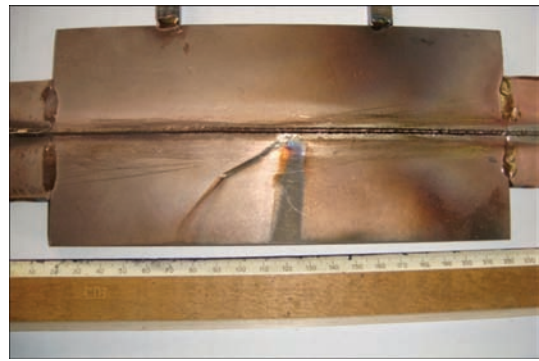


**Figure 2.** Welded joint of the pseudo- $\beta$  titanium alloy VT19, made by EBW on the side of weld root

The carried out examinations of the joints structure allowed concluding that in the weld metal produced at the welding speed of 7 mm/s the large, equiaxial polyhedral  $\beta$ -grains predominate. The weld metal consists almost of a pure  $\beta$ -phase (Figure 2, *b*) with hair-like boundaries, the amount of  $\beta$ -phase is 99 %.

The HAZ region, adjacent to the weld, which subjected to a complete polymorphic transformation, is not wide, its width is 2–3 grains. The region of a complete polymorphic transformation consists of an almost pure  $\beta$ -phase (Figure 3, *c*).

The strength of welded joints is at the level of 91 %, their structure is non-equilibrium and requires the use of heat treatment to produce a homogeneous uniform structure.

The weld metal of VT19 alloy, produced at the welding speed of 11 mm/s, also consists of equiaxial  $\beta$ -phase grains elongated in the direction of heat removal, whose boundaries are revealed on the background of the dendritic structure (Figure 3, *d*), in some of the weld metal grains, there are few disperse phase precipitations. The amount of  $\beta$ -phase decreased slightly and amounts to 92 %. The strength of the weld joint is at the level of 94 % of the base metal in the as-rolled state.

It should be noted that the microstructure of welded joint of VT19 alloy, produced at the speed  $v_w = 11$  mm/s, is similar to the microstructure of welded

**Table 1.** Properties of welded joints of titanium alloy VT19, produced by EBW

Number of specimen	Type of specimen; welding speed; heat treatment	$\sigma_t$ , MPa	$\sigma_y$ , MPa	$\delta$ , %	$\psi$ , %	KCV, J/cm <sup>2</sup>
1	Base metal; after rolling	958	887	12	47	27
2	Welded joint; 7 mm/s	876	842	11.3	36.8	29
3	Welded joint; 11 mm/s	890.7	847.0	10.0	45.9	28
4	Welded joint; 7 mm/s; preheating to 400 °C	893	879	12	47	21
5	Welded joint; 7 mm/s; preheating to 400 °C, LHT at 750 °C, 10 min	937	868	5.3	19	20
6	Welded joint; 7 mm/s; annealing at 750 °C, 1 h	1026.7	985.7	12.0	31.5	26
7	Welded joint; 11 mm/s; annealing at 750 °C, 1 h	1023.7	984.9	8.7	30.6	27
8	Welded joint; 7 mm/s; preheating to 400 °C, quenching in water and ageing at 450 °C	1285	1234	4.7	20.6	23

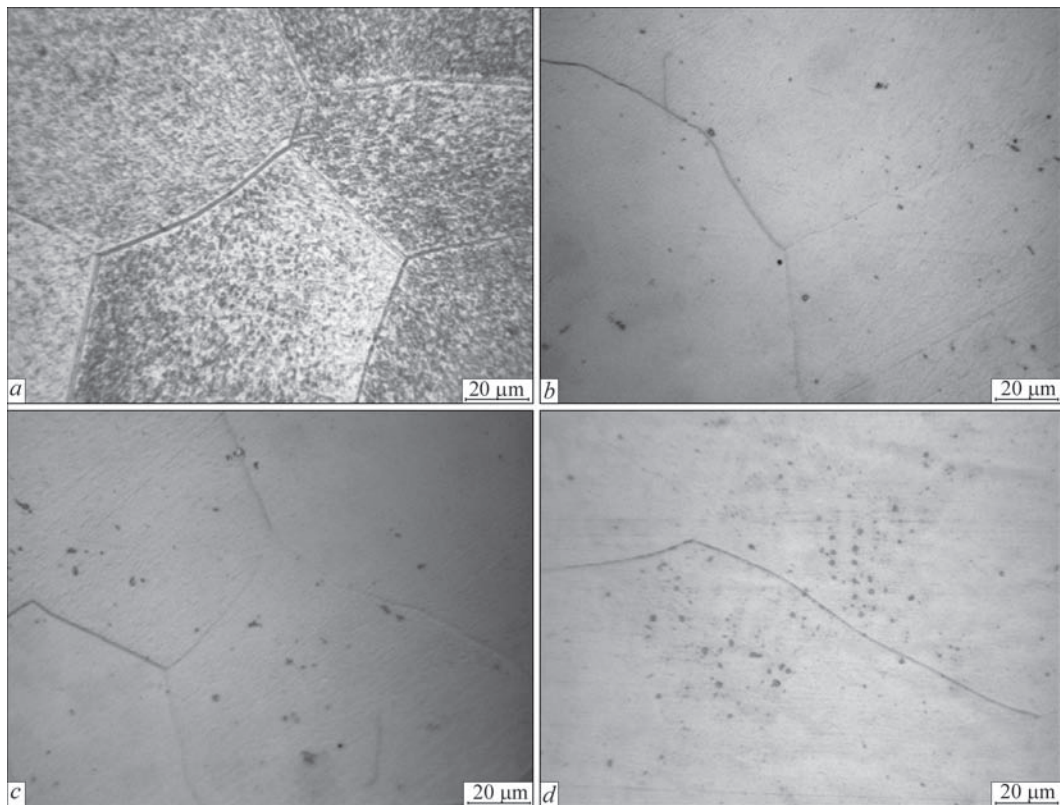


**Figure 3.** Microstructure of titanium alloy VT19 welded joint, produced by EBW, in the as-welded state: *a* — base metal; *b* — weld metal,  $v_w = 7$  mm/s; *c* — HAZ metal,  $v_w = 7$  mm/s; *d* — weld metal,  $v_w = 11$  mm/s

joint produced at the speed  $v_w = 17$  mm/s, despite the different speed of welding. Thus, after welding in the weld metal of welded joints, the  $\beta$ -phase is contained at the level of 92–99 %; the change in the welding speed does not allow changing the ratio between  $\alpha$ - and  $\beta$ -phases within the essential limits.

The weld metal of VT19 alloy, produced at the welding speed of 11 mm/s using a preheating of 400 °C, consists of equiaxial grains of  $\beta$ -phase elongated in the direction of heat removal and on the background of the dendritic structure. During application of preheating and as the result of decrease in the cooling rate of a welded joint in many grains of weld metal the irregularly distributed fine-dispersed

precipitations of other phase are fixed in a considerable amount (Figure 4, *a*), whose dimensions are less than 1  $\mu\text{m}$  (Figure 4, *b*). The amount of  $\beta$ -phase, as a result of applying preheating, decreased significantly and equals 60 %. This allows confirming the efficiency of a local preheating.

In the weld metal, produced by EBW using LHT (750 °C, 10 min), the amount of fine-dispersed precipitations of another phase is increased (Figure 5, *a*). The amount of  $\beta$ -phase as a result of preheating is decreased significantly and amounts to 53 %. The strength of welded joints is at the level of 99 % of the alloy strength itself. This allows making the conclusion that after LHT the amount of metastable  $\beta$ -phase

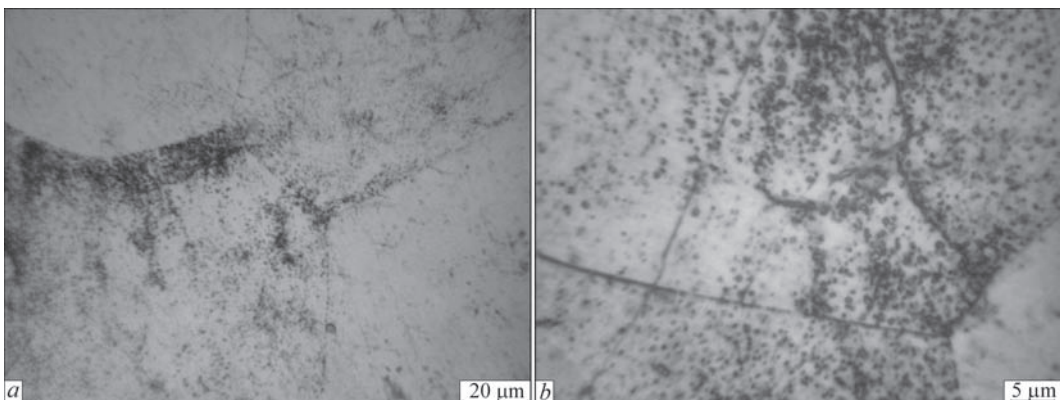


**Figure 4.** Microstructure of weld metal of titanium alloy VT19 welded joint, produced by EBW, in the as-welded state, at the speed of  $v_w = 7$  mm/s using preheating to 400 °C

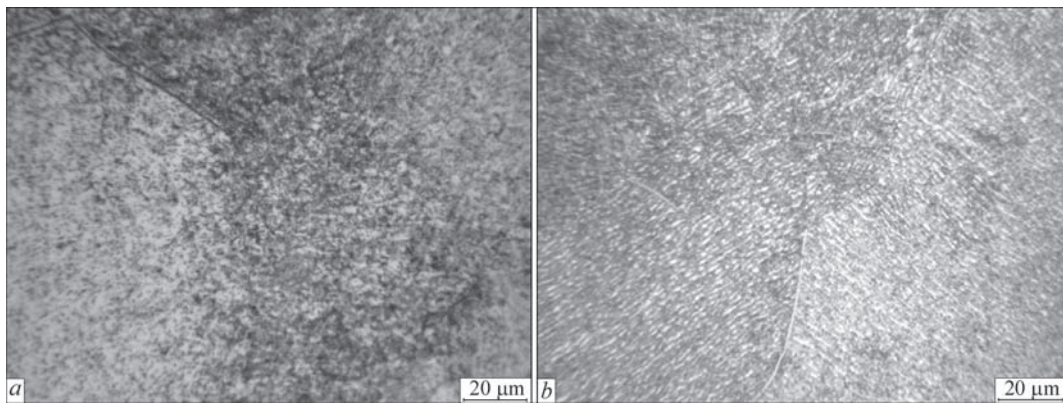


**Figure 5.** Microstructure of weld metal of titanium alloy VT19 welded joint, produced by EBW at the speed of  $v_w = 7$  mm/s using preheating to 400 °C: *a* — in the state after LHT at 750 °C, 10 min; *b* — after furnace annealing at 750 °C, 1 h

in weld metal decreases to a greater extent as compared to EBW with preheating to 400 °C only. The further increase in the strength of welded joints is limited by the strength of the base metal. Thus, the application of EBW in combination with preheating and LHT makes it possible to obtain the equal-strength welded joints of the titanium alloy VT19.

For comparison, a part of welded joints, produced at the welding speed of 7 mm/s, was subjected to furnace annealing at a temperature of 750 °C for 1 hour with the subsequent furnace cooling. The investigations showed that in this case the weld metal consists of equiaxial  $\beta$ -grains elongated in the direction of heat removal, which, as a result of annealing were subjected to decomposition with the formation of a uniform homogeneous two-phase structure (Figure 5, *b*) consisting of the particles of  $\alpha$  and  $\beta$ -phases. The particles of  $\alpha$ -phase have lamellar morphology, the length of  $\alpha$ -plates is 1–5  $\mu\text{m}$  at a thickness of 0.5–0.8  $\mu\text{m}$ . The amount of  $\beta$ -phase as a result of using furnace annealing is minimal for welded joints and is at the level of 35 %. The strength of welded joints in this case is maximal and amounts to 105–107 % of the strength of alloy in the as-rolled state. It should be noted, that the alloy VT19 allows using heat treatments at lower temperatures as compared with high-strength two-phase

alloys, such as VT23, T110 or T120 [7]. Thus, the annealing temperature is 750 °C, which is lower than the temperature of LHT being 850 °C or the temperature of recommended vacuum annealing of 900 °C for T120 alloy.

Thus, the application of EBW technology in combination with preheating and LHT allows producing the equal-strength welded joints of titanium alloy VT19, at the same time in order to produce a homogeneous uniform structure in all the zones of welded joint, it is necessary to apply a furnace annealing at the temperature of 750 °C for 1 h.

Since the strength of pseudo- $\beta$ -alloy VT19 in the wrought and hardened state can exceed 1500 MPa [8], and for high-strength titanium alloys and for pseudo- $\beta$ -alloy VT19 the quenching in water with the subsequent ageing is an effective hardening heat treatment [9–11], therefore, the feasibility of increasing the strength of joints, produced by EBW, was studied. For this purpose, a part of the specimens of number 2 (Table 1) was subjected to additional hardening heat treatment: quenching, which envisages heating to 800 °C, 1 h holding at 800 °C, quenching in water, ageing at 450 °C for 4 h.

The investigations of structure of the produced joints allowed making the conclusion that after hardening heat treatment consisting of quenching and subsequent ageing, the fine-dispersed decomposition

**Table 2.** Volumetric content of  $\beta$ -phase in BM and weld metal of titanium alloy VT19 welded joints, produced by EBW

Number of specimen	Type of specimen; welding speed; heat treatment mode	$\beta$ -phase, %
1	Base metal	44
2	Welded joint; 7 mm/s	99
3	Welded joint; 11 mm/s	92
4	Welded joint; 7 mm/s; preheating to 400 °C	60
5	Welded joint; 7 mm/s; preheating to 400 °C, LHT at 750 °C, 10 min	53
6	Welded joint; 7 mm/s; annealing at 750 °C, 1 h	34
7	Welded joint; 11 mm/s; annealing at 750 °C, 1 h	37

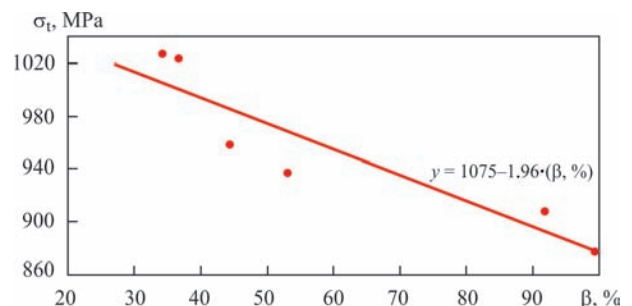


**Figure 6.** Dependence of strength of the joints, produced by EBW, on the amount of  $\beta$ -phase in the weld metal of titanium alloy VT19

products are formed in the weld metal and HAZ metal of this welded joint, the size of which is mainly amounts to 1.0–1.5  $\mu\text{m}$ .

The carried out investigations allowed making a conclusion that as a result of quenching and subsequent ageing, in welded joints of VT19 alloy, produced by EBW, the most fine-dispersed intragranular structure of weld metal is formed, in which the size of decomposition products more often does not exceed 1  $\mu\text{m}$ , in the HAZ the size amounts to 1–1.5  $\mu\text{m}$ . The fine-dispersed structure in all the zones of welded joint of VT19 alloy provides it with high strength, reaching  $\sigma_t = 1285 \text{ MPa}$ , at high impact strength  $KCV = 23 \text{ J/cm}^2$ .

It should be noted that for welded joints of titanium pseudo- $\beta$  VT19 alloy, the effective hardening heat treatment is quenching into water with subsequent ageing, which provides the strength of the joints at the level of 130 % of strength of the alloy in as-rolled state.

The investigations of microstructure of produced welded joints and their comparison with the results of evaluation of mechanical properties of joints allowed establishing the inverse dependence of strength of the titanium pseudo- $\beta$  VT19 alloy joints, produced by EBW on the amount of  $\beta$ -phase in the weld metal (Figure 6). This dependence has the form  $\sigma_t = 1072 - 1.96 (\beta, \%)$ , according to which the minimum values of strength of welded joints ( $\sigma_t = 881 \text{ MPa}$ ) are obtained at the 99 % content of  $\beta$ -phase, and the maximum values ( $\sigma_t = 1054 \text{ MPa}$ ) are obtained at the 25 % content of  $\beta$ -phase.

## Conclusions

1. The variation of speed of EBW of VT19 alloy does not allow changing significantly the ratio between  $\alpha$ - and  $\beta$ -phases in the weld and HAZ metals, the structure of joint, made at speed of 11 mm/s is similar to the structure of joint, produced at speed of 7 mm/s.

2. EBW in combination with preheating allows regulating the ratio between  $\alpha$ - and  $\beta$ -phases in the welded joint metal and reducing the content of  $\beta$ -phase in the weld metal of VT19 alloy from 91 to 53 %, increasing the strength of welded joints from 876 up to 937 MPa and, as a result, providing the strength of welded joints, equal to that of base metal.

3. To form the homogeneous structure, increase the strength of base and welded joint metals up to 1020 MPa level, provide complete decomposition of metastable phases, the joints of VT19 alloy should be subjected to furnace annealing at the temperature of 750 °C for 1 h, as a result of which the strength level of the joints is increased to 105–107 % of that of the alloy after rolling.

4. The quenching in water with next ageing provides high strength values of the joint of VT19 alloy at the level of 1285 MPa. In this case a fine-grained intragranular structure is formed in the weld and HAZ metal, in which the size of  $\alpha$ -phase particles does not exceed 1.5  $\mu\text{m}$ .

1. Kablov, E.N. (2012) Strategic directions of development of materials and technologies of their recycling from the period up to 2030. *Aviats. Materialy i Tekhnologii*, **S**, 7–17 [in Russian].
2. Khorev, A.I. (2012) Titanium super alloy VT19. *Tekhnologiya Mashinostr.*, **6**, 5–8 [in Russian].
3. Gurevich, S.M., Zamkov, V.N., Blashchuk, V.E. et al. (1986) *Metallurgy and technology of welding of titanium and its alloys*. Kiev, Naukova Dumka [in Russian].
4. Lyasotskaya, V.S., Lysenkov, Yu.T., Biryukov, I.M. et al. (1981) Improvement of properties of welded joints of VT9 alloys by local electron beam heat treatment. *Svarochn. Proizvodstvo*, **11**, 19–20.
5. Lyasotskaya, V.S., Lysenkov, Yu.T., Gerasimenko, A.V. et al. (1985) Influence of local heat treatment on structure and properties of welded joints of VT6ch alloy. *Aviats. Promyshlennost*, **11**, 57–59 [in Russian].
6. Vrzhezhevsky, E.L., Sabokar, V.K., Akhonin, S.V. et al. (2013) Influence of local heat treatment at EBW of titanium alloys with silicide strengthening on mechanical properties of weld metal. *The Paton Welding J.*, **2**, 20–23.
7. Akhonin, S.V., Belous, V.Yu., Selin, R.V. et al. (2015) Structure and properties of EB- and TIG-welded joints of high-strength two-phase titanium alloys. *Ibid.*, **8**, 14–17.
8. Khorev, A.I. (2009) Development of structural titanium alloys for manufacture of components of aerospace engineering. *Svarochn. Proizvodstvo*, **3**, 13–23 [in Russian].
9. Gavze, A.L., Petrova, E.N., Chusov, S.Y., Yankov, V.P. (2009) Investigation of properties of titanium alloys with mechanically stable beta-structure for body armor application. *Techniczne Wybory Wlokiennicze*, **17(2/3)**, 54–57.
10. Popov, A.A., Illarionov, A.G., Oleneva, O.A. (2010) Structure and properties of welded joints from high titanium alloy after heat treatment. *Metallovedenie i Termich. Obrab. Metallov*, **10**, 23–27 [in Russian].
11. Luetjering, G., Albrecht, J. (eds) (2003) Ti-2003 Science and Technology. In: *Proc. of the 10th World Conf. on Titanium (13–18 July 2003, Hamburg, Germany)*, 385, 2643, 3035.

Received 01.06.2018

## ON THE PROBLEM OF MODELING TRANSVERSE MAGNETIC FIELD STRUCTURE IN WELDING POOL ZONE

A.D. RAZMYSHLYAEV<sup>1</sup>, P.A. VYDMYSH<sup>2</sup> and M.V. AGEEVA<sup>3</sup>

<sup>1</sup>State Higher Educational Institution «Pryazovskyi State Technical University»  
7 Universitetskaya Str., 87500, Mariupol, Ukraine. E-mail: razmyshljaey@gmail.com

<sup>2</sup>OJSC «Metinvest-Promservis»

113-a Nikopol Ave., 87500, Mariupol, Ukraine, E-mail: pstukmu@gmail.com

<sup>3</sup>Donbass State Machine Building Academy

72 Akademicheskaya Str., 84313, Kramatorsk, Ukraine. E-mail: maryna\_ah@ukr.net

It was established experimentally that a normal component of induction along the side surfaces of rods of the input device of the transverse magnetic field is distributed almost uniformly (has the same values). A slight increase in the values of this induction component is observed only in the zones at the ends of rods and coils, placed on these rods. To study the distribution of transverse magnetic field induction in the welding pool zone (at the base metal surface), it was proposed to use the well-known assumption that there is an analogy between the structure of magnetostatic and electrostatic fields. On this basis, a procedure was proposed which allows calculating the distribution of transverse and longitudinal induction components of the magnetic field generated by the input device of the transverse magnetic field at the surface of welded plate of nonmagnetic materials. In this case, the known equations of electrostatics are used. It was assumed in the calculations that charges of electrostatic field on the side surfaces and rod ends of the input device of the transverse magnetic field are uniformly distributed. It is shown that the proposed method provides a satisfactory convergence of calculated and experimental data. 8 Ref., 6 Figures.

**Keywords:** *transverse magnetic field, induction, Coulomb's law, electrostatic field strength*

The use of a transverse magnetic field (TMF) in arc welding and surfacing provides the control of welds (beads) geometry, increase in the coefficient of electrode melting and refinement in structure of welds (deposits) [1–4].

The study of TMF structure in the weld pool zone has a theoretical and practical importance. However, there are no simple procedures for calculating the induction of the magnetic field, generated by two-rod systems of TMF input devices (ID) in the weld pool zone.

The well-known calculation program ANSYS provides determination of the induction values generated by the TMF ID in this zone. However, its use is hindered because of excessive complexity [5]. The excessive complexity is also inherent in a calculation procedure based on the use of a method of secondary sources, when a numerical solution of the problem by the finite element method is also required [6, 7]. It is necessary to develop a calculation procedure which is simpler in use.

According to the literature data [6], there is an analogy between the structure of the magnetic field generated by the TMF ID and the structure of the electrostatic field, if the latter field was generated by the similar charged bodies. According to the data present-

ed, in particular, in work [6], at a certain point of the surrounding space, the induction  $B$  and the electric field intensity  $E$ , generated respectively by electromagnets and charged bodies, are summed as vectors. The mathematical apparatus for describing the structure of the electrostatic field was developed more fully unlike that for the electromagnetic field. It should be noted that as-applied to calculation of induction of the magnetic field generated by the TMFID, this method was not used.

The aim of this work is to analyze the feasibility of modeling a stationary magnetic field, generated by the TMF ID, using a stationary electrostatic field in the pool zone during arc welding and surfacing.

Below the developed calculation method of modeling the spatial distribution of the induction of the controlling TMF in the zone of the weld pool is presented by using the equations of electrostatics.

Investigated were the features of structure of the magnetic field generated by a single rod with winding. The cross-section of the rod of low-carbon steel was  $F_s = 26 \times 16$  mm, the rod length was  $L_f = 130$  mm. On the rod a winding of a copper wire of 1.0 mm diameter was arranged with a number of coils  $W = 100$ . The winding was four-layered and had a height of 30 mm. The winding was positioned in the rod length center.

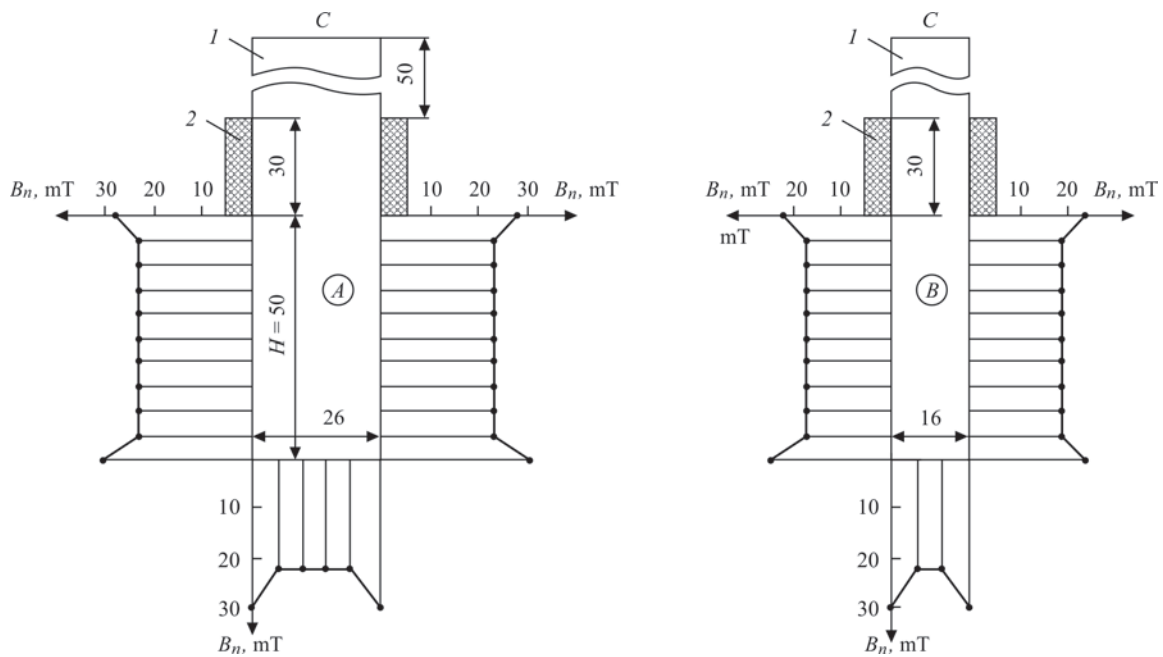


**Figure 1.** Distribution of induction  $B_n$  along the surfaces of rod ( $W = 100$ ,  $I_c = 8$  A): 1 — rod; 2 — winding

The normal induction component  $B_n$  and also the induction component  $B_n$  normal to the rod end at the section below the winding were measured along the side surfaces of the rod. In the coil, a direct current  $I_c = 8$  A was passed. The measurements of induction  $B_n$  were performed applying a milliteslameter of type 43205 with a Hall sensor having a measuring base of  $0.9 \times 0.9$  mm. The measurement data are shown in Figure 1. The data demonstrated a «splash» of induction  $B_n$  only at the winding end and below at the rod end. A «splash» of  $B_n$  was observed in the sections of about 5 mm length, while along the entire length of the rod and at its end the induction  $B_n$  was distributed rather uniformly. The tangent component of magnetic field

induction on all the rod surfaces was almost equal to zero. The similar data were obtained using rods of  $26 \times 32$  mm and  $32 \times 52$  mm section. With a decrease in the distance from the coils up to the rod ends from 60 to 20 mm, the nature of change in the induction components corresponded to that preset for the rod of  $26 \times 16$  mm section (Figure 1). This statement was also preserved for the rods, made as a set of plates of electrical steel E42 of 0.5 mm thickness.

To develop the calculation procedure, the magnetized section of the rod (below the winding) was replaced by a dielectric body, having charges on its surface. The dimensions of such a dielectric body are the same as the considered section of the electromagnet rod. Moreover, the charges on the surfaces (A, B, C) of the indicated body were distributed uniformly.

As an example, Figure 2 shows dividing of surfaces into sections of the same area, at the center of which the charges  $q$  are arranged. It is necessary that all the small sections (after dividing) on all the side surfaces and ends of the rods (A, B, C in Figure 2) have the same area. It is rational to start dividing of the rod (C) ends area into sections. The sufficient quantity of areas on the surfaces C is 8–12. The larger the quantity of sections, the more accurate the results of calculations will be in future. However, the amount of calculation works will increase.

As is known [6], according to Coulomb's law, the intensity of the electrostatic field  $E$  from the charge  $q$  in a point at the distance  $R$  from the charge:

$$E = \frac{q}{4\pi\epsilon_0 R^2} \quad (1)$$

where  $\epsilon_0$  is the electric constant;  $\epsilon_0 = 8.85 \cdot 10^{-12}$  F/m.

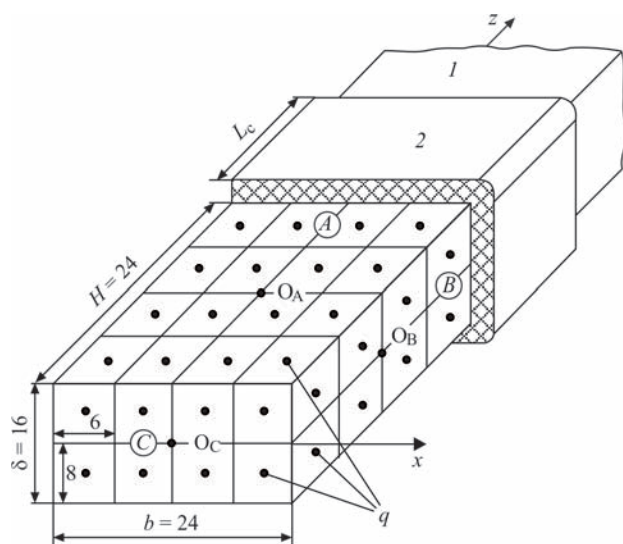


**Figure 2.** Scheme of distribution of charges at the surfaces A, B, C of the rod (1) below the level of the coil (2);  $H$ ,  $b$ ,  $\delta$  — dimensions of the rod area (m);  $L_c$  — length of the coil (m); (points — places of charges arrangement)

Since  $q/(4\pi\epsilon_0) = \text{const}$ , then in the formula (1) to estimate (calculate)  $E$ , generated by a charge on the side surface of the TMF ID, any numerical value  $q/(4\pi\epsilon_0) = K$  (convenient for calculations) can be taken.

Then the formula (1) will take the form:

$$E = \frac{K}{R^2}. \quad (2)$$

The calculation by formula (2) is convenient, because in order to finally evaluate the character of distribution, the field intensity  $E (E_x, E_y, E_z)$  along any direction (axes  $X, Y, Z$ ) should be expressed in relative units, for example, through the parameter  $E_x/E_{x\text{max}}$ . In this case, the distribution of the electrostatic field component  $E_x/E_{x\text{max}}$  can be compared with the distribution of induction components of the magnetic field generated by the real structure of the TMF ID ( $B_x/B_{x\text{max}}$ ). In addition, the values of components of field  $E (E_x, E_y, E_z)$  along any direction allow evaluating numerically (in divisions, units, obtained during the calculation) the influence of dimensions and arrangement of the TMF ID rods in space, the inclination of rods to the vertical axis on the value of field components  $E (E_x, E_y, E_z)$ , and, thus, allows determining the optimal parameters of the TMF ID, providing the maximum values of components of the field  $E_x, E_y, E_z$  at a certain point (analogues of values of components of the magnetic field  $B_x, B_y, B_z$  in the point).

It was established earlier [8] that the structure of a controlling TMF generated by different structures of  $\Pi$ -type ID in relative units does not depend on how the magnetic force lines of are closed at the upper part of the two-rod TMF ID systems. This was the basis for modeling the magnetic field by the electrostatic field for the TMF ID from two rods (with windings), not connected by a jumper at the top.

In the calculations, the lower part of two rods with a section  $F_s = b \times \delta = 26 \times 16$  mm, of length  $H = 50$  mm in the zone below the coils was considered. On the surfaces of rods, the point-like charges of the same size were arranged (in Figure 3, in the form of points the charges are indicated arranged on the vertical surfaces of each of the two rods, but the similar charges are also arranged on the lower ends of rods).

The vectors  $E$  of each charge are decomposed in space into three components directed along the coordinate axes  $OX, OZ, OY$  through the cosines of direction angles  $\alpha, \beta, \gamma$  of vector  $E$  with respect to these axes (Figure 4).

It was assumed that from each charge on the surface A of the rod, positive pole (+), the vector of the field intensity  $E$  «comes out», and the vector  $E'$  «comes in» the same point of the rod B, negative pole (-) (see Figure 3).

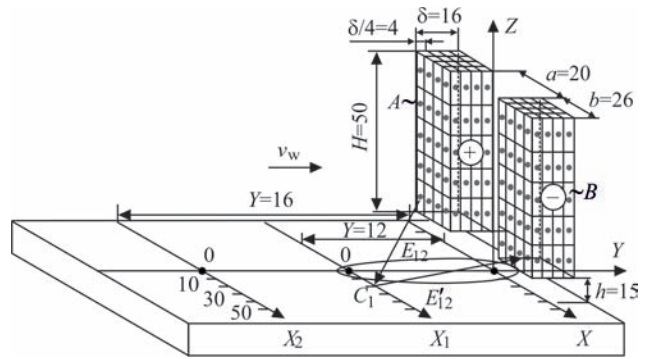


Figure 3. Scheme for the calculation of vector  $E$  in the point  $C_1$  at the plate surface

For each vector of intensity, the following equations can be composed:

$$E_{Y_i} = E \cos \beta = E_i \frac{y_i}{R_i}, \quad (3)$$

$$E_{Z_i} = E \cos \gamma = E_i \frac{z_i}{R_i}, \quad (4)$$

$$E_{X_i} = E \cos \alpha = E_i \frac{x_i}{R_i}, \quad (5)$$

where  $E$  is the value of the field intensity at the point considered,

$$E = \frac{q}{4\pi\epsilon_0\epsilon_r R^2}, \quad (6)$$

$y_i, z_i, x_i$  is the length of vector  $E$  projection to the corresponding axis, m;  $R_i$  is the distance from the charge  $q_i$  to the point considered  $C_1$ , m.

Further, the calculation was carried out according to the formula (2), where  $K$  is a constant value:

$$K = \frac{q_i}{4\pi\epsilon_0\epsilon_r} = \text{const}. \quad (7)$$

To obtain the numerical values of the vectors  $E_x, E_y, E_z$ , at a given point of space (in particular, at the point  $C_1$ ), the summation of all the components  $E'_{xi}, E'_{yi}, E'_{zi}$  was performed at this point from each charge  $q_i$  arranged on the surfaces A and B of rods and at the end C.

Moreover, the bodies (rods A and B in Figure 3) are considered conditionally opaque, i.e. it is necessary to take into account the action of only those charges  $q$  on

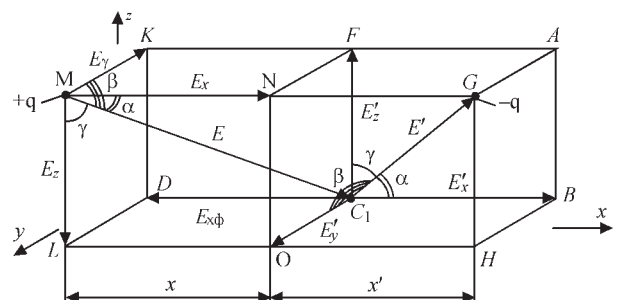
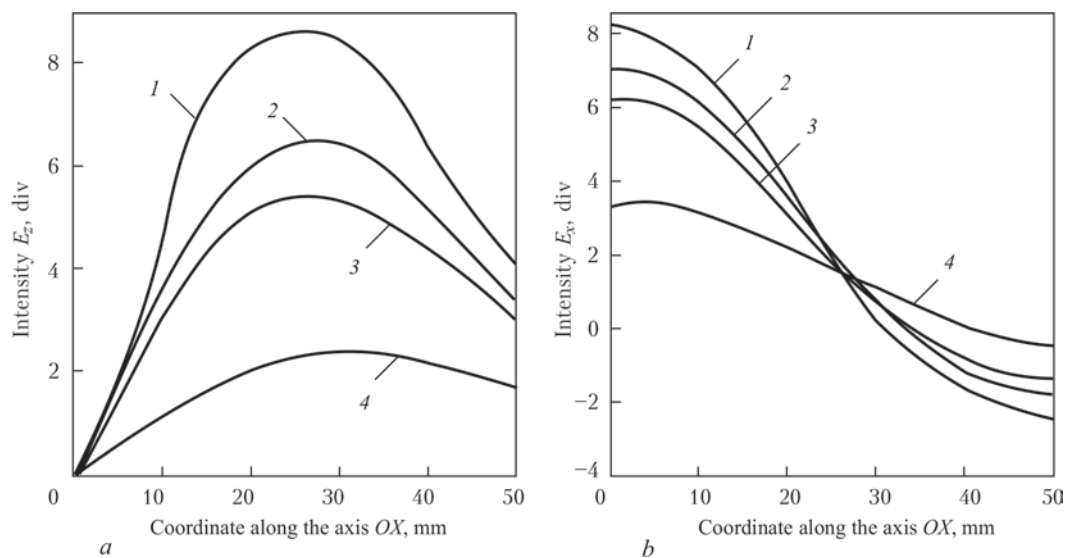


Figure 4. Scheme of disintegration of vector  $E$  in the space into its components parallel to the axes  $X, Y, Z$



**Figure 5.** Distribution of calculation values  $E_z$  (a) and  $E_x$  (b) along the axes  $OX$ : 1–4 — respectively, at  $y = 0; 12; 16; 32$  mm

the surfaces  $A, B$  and  $C$  of rods which are «visible» from the point  $C_1$ .

To evaluate the feasibility of practical application of the proposed calculation procedure, it is necessary to compare the calculated data with the corresponding experimental data. For this purpose, the distribution of components  $B_z, B_x$  of the magnetic fields, generated by the real TMF ID, were investigated. In the investigations, the electromagnets with a cross-section of rods of low-carbon steel  $F_s = b \times \delta = 26 \times 16$  mm, length  $L = 130$  mm with windings of length  $l = 30$  mm were used. The distance from the windings to the rod end is  $H = 50$  mm. Through the coils a direct current  $I = 8$  A was passed. The induction was measured by a universal 43205 teslameter with a Hall sensor having a base of  $0.9 \times 0.9$  mm.

To evaluate the structure of the magnetic field in the pool, a calculation scheme of two rods  $F_s =$

$= 26 \times 16$  mm and a conditional distribution of charges along the side surfaces were taken, shown in Figure 3. The distance between the rods was  $a = 20$  mm; between the axis  $OX$  (surface of the product) and the rod ends it was  $h = 15$  mm. The inclination angle of rods to vertical was  $\alpha = 0^\circ$ . The calculations were carried out taking into account the actions of all charges on the surfaces of all the rods ( $A, B$  and  $C$ ), which are «visible» from the point  $C_1$ . To accelerate the calculations the program Mathcad 15 was used.

The absolute values of the field intensity  $E$  at the points arranged along the axis  $OX$  with a step of 10 mm, with the coordinates along the axis  $OY$  in the direction opposite to the welding direction,  $Y_0 = 0$  mm,  $Y_1 = 12$  mm,  $Y_2 = 16$  mm and  $Y_3 = 32$  mm were determined (Figure 3). In the calculation, the dependence  $E = 16/R^2$  ( $R$  was measured in cm) was used. In this case, the numbers are obtained which are

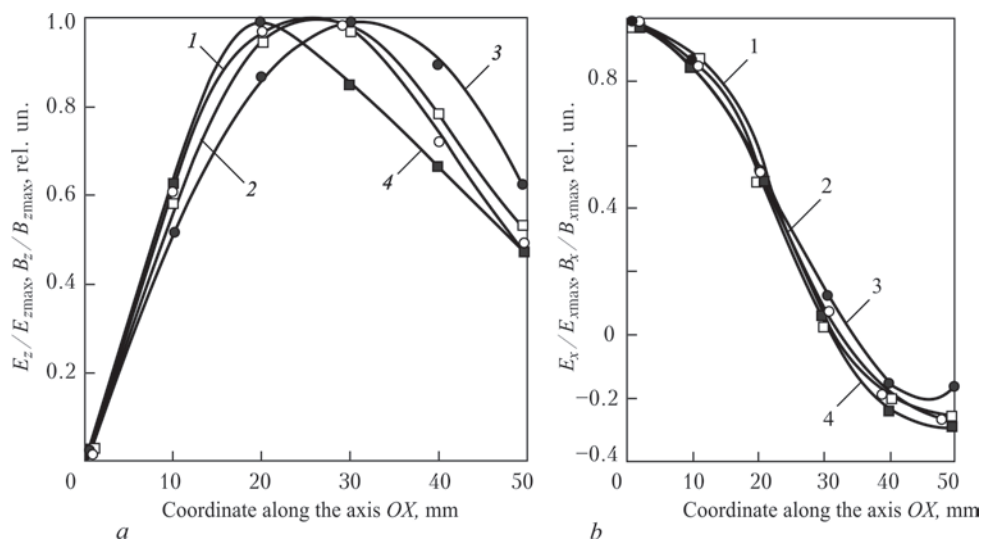


**Figure 6.** Distribution of relative values  $E_z/E_{zmax}, B_z/B_{zmax}$  (a) and  $E_x/E_{xmax}, B_x/B_{xmax}$  (b) along the axes  $OX$ : 1–4 — respectively, at  $y = 0; 12; 16; 32$  mm (in lines the calculation relative values for  $E_z/E_{zmax}$  (a) and  $E_x/E_{xmax}$  (a) and  $E_x/E_{xmax}$  (b) are indicated; in marks the experimental data for  $B_z/B_{zmax}$  (a) and  $B_x/B_{xmax}$  (b))

analogous to the values of the components of electrostatic field intensities  $E_z, E_x$ . In principle the numerical values  $E_z, E_x$  (in divisions) correspond to the values  $E_z, E_x$ , having the dimension B/m.

The data showed that the nature of distribution of calculated values of the longitudinal and transverse components  $E_z$  and  $E_x$  (analogous of the components of inductions  $B_z$  and  $B_x$ ) along the axes  $OX$  is preserved with increasing distance along the axis  $OY$  (see Figure 3) in the direction opposite to the direction of welding (Figure 5, *a* and *b*). The calculated relative values  $E_z/E_{z_{\max}}$  and  $E_x/E_{x_{\max}}$  shown in Figure 6, *a* and *b*, corresponding to the experimental relative ratios of inductions  $B_z/B_{z_{\max}}$  and  $B_x/B_{x_{\max}}$  for real rods of the TMF ID almost coincide with each other.

Thus, the proposed method provides a satisfactory convergence of calculation data on the distribution of components of intensity of the modeling electrostatic field and the experimental data on the distribution of the magnetic field induction components in the weld pool zone. The method can be used to optimize the structure of the TMF ID to provide maximum values of the transverse induction component in the weld pool zone at a constant value of the magnetizing force of windings at the rods of this ID.

It should be noted that all the results of investigations mentioned above relate to the case when the product is not made of ferromagnetic material. To obtain the numerical values of the induction components shown in Figure 6 in the form of their relative values, it is necessary to know their numerical values for at least one point in this diagram. The method of calculated determination of numerical values of induction components, generated by the TMF ID, will be presented in the next publication.

## Conclusions

1. A calculation procedure was proposed using the equations of electrostatics, which adequately reflects the structure of the magnetic fields generated by real TMF ID and allows estimating the distribution of the MF induction components in the weld pool zone.

2. The proposed method can be used to optimize the structure of the TMF ID to provide the maximum values of the transverse induction component in the weld pool zone at the unchanged value of magnetizing force of windings at the rods of this ID.

1. Skipersky, N.A., Rybachuk, A.M. (2000) Weld formation by transverse magnetic field in welding of nonmagnetic materials. *Svarochn. Proizvodstvo*, **7**, 53–55 [in Russian].
2. Iofinov, P.A., Ibragimov, V.S., Dmitrienko, A.K. et al. (1991) Influence of external electromagnetic field on melting rate of electrode wire in submerged-arc welding. *Ibid.*, **1**, 34–35 [in Russian].
3. Razmyshlyayev, A.D., Mironova, M.V., Kuzmenko, K.G. (2011) Efficiency of melting of electrode wire in submerged arc surfacing with influence of transverse magnetic field. *The Paton Welding J.*, **5**, 39–42.
4. Ryzhov, R.N., Kuznetsov, V.D. (2006) External electromagnetic effects in arc in processes of arc welding and surfacing (Review). *Ibid.*, **10**, 29–35.
5. Andreeva, E.G., Shamets, S.P., Kolmogorov, D.V. (2005) Calculation of stationary magnetic fields and characteristics of electric devices using program package ANSYS. *Electronic Sci. J. Oil and Gas Business*, **1**. [http://ogbus.ru/authors/Andreeva/Andreeva\\_1.pdf](http://ogbus.ru/authors/Andreeva/Andreeva_1.pdf).
6. Bessonov, L.A. (2003) *Theoretical fundamentals of electrical engineering. Electromagnetic field*. Moscow, Gardariki [in Russian].
7. Tozoni, O.V. (1975) *Method of secondary sources in electrical engineering*. Moscow, Energiya [in Russian].
8. Razmyshlyayev, A.D., Mironova, M.V., Yarmonov, S.V. et al. (2013) Structure of transverse magnetic field generated by input devices for arc welding process. *Visnyk Pryazov. DTU: Transact. Mariupol, PDTU*, 135–141 [in Russian].

Received 29.05.2018

# TECHNICAL PARAMETERS AND FEATURES OF MANUFACTURING HIGH-PRESSURE VESSELS FOR NATURAL GAS TRANSPORTATION

V.M. KULIK

E.O. Paton Electric Welding Institute of the NAS of Ukraine  
11 Kazimir Malevich Str., 03150, Kyiv, Ukraine. E-mail: [office@paton.kiev.ua](mailto:office@paton.kiev.ua)

Considered are the technical capabilities of simplified manufacture of all-metal high-pressure vessels for delivery of natural gas through application of prefabricated 351–610 mm pipes from higher strength steels. Dimension-weight parameters and stresses in the vessel wall, depending on steel strength, are determined. The structure, structural-mechanical inhomogeneity and fatigue resistance of the welded joints were examined. Elimination of rolling, welding, thermomechanical treatment, heat treatment of the shell from the technological process and formation of outer fiberglass casing, as well as reduction of wall thickness, diameter and weight provides significant simplification of vessel manufacture, reduction of the number of passes, time of welding the circumferential welds, and power consumption. 25 Ref., 1 Table, 5 Figures.

**Keywords:** *all-metal high-pressure vessels, pipes, stresses, welded joints, structure, mechanical properties, cyclic fatigue life, dimension-weight characteristics*

One of the kinds of natural gas delivery is its marine transportation by ships under the pressure of 20–30 MPa in cylindrical steel and metal plastic vessels, made with application of gas pipes of a large diameter (1020, 1029, 1067, 1219 mm) with up to 40 mm wall thickness from steel of X80 grade [1–5]. It is proposed to perform gas delivery to Ukraine in metal plastic vessels of 390 and 1020 mm diameter and 5.8 and 11.7 m length [1, 6]. They are manufactured with application of rolling, welding of longitudinal joints, thermomechanical and heat treatment of the shell from 30KhGSA steel [7], or using X80 steel pipes [8] and forming the outer fiberglass casing. Application of large diameter pipes from high-strength low-alloyed steels was proposed for manufacturing metal plastic vessels for rapid supply of compressed gases to small enterprises, farms, etc. [9].

In view of the possible instability of gas imports, it is urgent to arrange delivery of natural gas in simplified mobile vessels, production of which can be quickly mastered. Manufacturing all-metal large diameter vessels with greater wall thickness and metal plastic vessels reinforced by fiberglass casing of approximately three times greater thickness than that of the body wall [10], is quite complicated for the modern technical condition of Ukrainian industry.

The objective of the work was determination of the feasibility and evaluation of the effectiveness of simplified manufacture of high pressure vessels for delivery and storage of natural gas with the prospect of possible rapid mastering of their production. It is achieved by elimination from the technological process of forming of the fiberglass casing and manufac-

turing of the heat-treated shell due to application of prefabricated pipes of medium diameter, including heat-treated pipes, with wall thickness not greater than that of the wall (9.1 and 13.5 mm) of the bodies of metal plastic vessels of a large diameter (1020 mm).

An all-metal vessel consists of equal-thickness shell of medium diameter pipe from higher strength steel and two convex bottoms with branch pipe and union, in at least one of them, which are butt welded by circumferential welds. Pipes of 426 mm and greater diameter, produced in Ukraine with application of arc welding, can be manufactured from sheet steels of X80 and X100 grade. Such steels, alloyed by 1.6–1.9 % Mn and microalloyed with Ni, Cr, Mo, Ti, V, Nb, after thermomechanical treatment, including controlled rolling and accelerated cooling, as well as other kinds of treatment, are characterized by higher strength ( $\sigma_t \geq 625$  and 760 MPa), ductility ( $\delta_5 \geq 18$  and 17 %) and toughness ( $KC_{-40} \geq 155$  and 160 J). Lowering of the content of carbon to 0.03 % and of sulphur to 0.01 % ensures increase of ductility, deformability and toughness, and improvement of weldability, compared to alloyed carbon steel [11–13].

Seamless hot-deformed pipes of 530 (550) mm and smaller diameter are manufactured from 30KhGSA steel with  $\sigma_t \geq 686$  MPa and  $\delta_5 \geq 11$  %. At customer's request they shall be made heat-treated. Such pipes are given in the list of materials, used for manufacturing pressure vessels [14].

The main technical parameters of the considered all-metal vessels 11.4–11.6 m long, proposed for natural gas delivery (as a possible variant), are given in the Table. They were determined with application of formu-

Dimension-weight parameters and stresses in the wall of steel vessels of 11.4–11.6 length at  $P_w = 20$  MPa

Parameters	Pipe and vessel steel											
	X80 $\sigma_t = 640$ MPa		30KhGSA with HT $\sigma_t = 960$ MPa		30KhGSA without HT $\sigma_t = 700$ MPa				X100 $\sigma_t = 800$ MPa			
$D$ , mm	508	426	530	508	530	426	377	351	610	558	508	426
$S$ , mm	13.2	11.1	9.4	9.0	12.7	10.2	9.0	(8.5)	12.8	11.7	10.7	9.0
$D/S$	38.5	38.4	56.4	56.4	41.7	41.8	41.9	41.3	47.6	47.7	47.5	47.3
$K$	1.75	1.75	1.76	1.76	1.76	1.76	1.75	1.78	1.75	1.75	1.76	1.76
$[\sigma]$ , MPa	365.7	365.7	545.5	545.5	397.7	397.7	400.0	392.9	457.1	457.1	454.5	454.5
$\sigma_w^h$ , MPa	364.8	363.8	543.8	544.4	397.3	397.6	398.9	392.0	456.6	456.9	454.7	453.2
$\sigma_w^m$ , MPa	177.5	177.1	267.0	267.3	193.8	193.9	194.6	191.6	223.4	223.6	222.5	221.7
$V$ , m <sup>3</sup>	2.06	1.44	2.33	2.14	2.27	1.45	1.14	0.985	3.06	2.55	2.11	1.47
$M$ , t	1.85	1.29	1.40	1.28	1.86	1.19	0.93	0.814	2.19	1.82	1.50	1.05
$M/V$ , t/m <sup>3</sup>	0.89	0.89	0.60	0.60	0.81	0.82	0.81	0.826	0.71	0.71	0.71	0.71

las (1)–(5), of which formulas (2)–(3) are given in work [15], and formula (1) is derived from formula (2).

$$S = \frac{K_s P_w D}{2(\sigma_w + K_s P_w)}, \quad (1)$$

$$\sigma_w^h = \frac{P_w (D - 2S)}{2S}, \quad (2)$$

$$\sigma_w^m = \frac{P_w (D - 2S)}{4(D - S)}, \quad (3)$$

$$V = 0.262(D - 2S)^2(3l_c + 2D), \quad (4)$$

$$M = 24.65S(D - S)(l_c + D), \quad (5)$$

where  $S$ ,  $D$  and  $l_c$  are the wall thickness, outer diameter and length of the vessel cylindrical part;  $K_s$  is the coefficient of safety of the vessel;  $P_w$  is the working pressure of gas in the vessel (20 MPa);  $\sigma_w^h$ ,  $\sigma_w^m$  and  $[\sigma]$  are the working hoop, meridian and allowable stresses in the wall;  $V$  and  $M$  are the capacity and weight of the vessel.

According to DNV Rules for cargo tanks of CNG ships  $K_s = 1.60$ – $1.80$  is allowed [3].  $K_s$  value can be the same for the main pipelines, and at wall thickness of 18.7 mm with a surface defect of 500 mm length and up to 5.3 mm depth it is equal to 1.77–1.80 [16]. Metal plastic vessels are allowed to be manufactured with  $K_s = 1.70$  and 1.75 [1, 17]. Therefore, keeping the safety coefficient of approximately 1.75 for all-metal welded vessels is completely justified.

Minimum diameter of vessels from X80 and X100 steels, given in the Table, is determined by minimum diameter of 426 mm of pipes manufactured in Ukraine with application of arc welding. Calculated wall thickness of 9.0 and 8.5 mm corresponds to minimum diameters of 508 and 351 mm of vessels from 30KhGSA steel. Seamless hot-deformed pipes (heat-treated and non-heat treated) of the given diameters with wall thicknesses smaller than those given above, are not manufactured. In vessels of greater diameters than those

given in the Table, wall thickness exceeds that of the body from the same steel in metal plastic vessels.

At application of pipes from X80 steel the vessel wall thickness with the coefficient of safety of 1.75 can be 11.1 and 13.2 mm. Wall thickness of vessels from heat-treated and non-heat treated 30KhGSA steel and X100 steel can be 9.0–9.4; 8.5–12.7 and 9.0–12.8 mm, respectively, keeping the coefficient of safety of 1.75–1.78. Here, vessels from the two latter steels are manufactured in a broader range of diameters of 351–530 and 426–610 mm. Vessel  $D/S$  ratio grows linearly with increase of steel  $\sigma_t$ , which is accompanied by decrease of  $M/V$  ratio from 0.89 to 0.60 t/m<sup>3</sup> (Figure 1). A similar reduction of  $M/V$  occurs almost linearly with  $D/S$  increase. Here, the vessels from steel of the same level of strength have the same  $D/S$ ,  $\sigma_w^h$ ,  $\sigma_w^m$ , and  $M/V$  values.

Working hoop stresses  $\sigma_w^h$  do not exceed allowable stresses  $[\sigma] = \sigma_t/K_s$ , and meridian stresses  $\sigma_w^m$  are lower than  $[\sigma]$  2.04–2.06 times. This eliminates vessel destruction at a constant gas pressure of 20 MPa. Stresses in the wall of hemispherical bottoms are the same as meridian stresses [15]. Therefore, the bottoms can be formed from less expensive unalloyed and low-alloyed widely applied steels, which are used for manufacturing pressure vessels. Their  $\sigma_t$  should not be lower than  $0.5\sigma_t$  of the applied pipe steel.

The weight of all-metal vessels in the range of 0.81–1.85 t is much smaller than  $M = 4.95$  and 6.15 t of metal plastic vessels of the same length. This, in combination with smaller wall thickness and diameter, facilitates performance of welding and rigging operations. Their capacity of 0.99–3.06 m<sup>3</sup> is much lower than that of metal plastic vessels of a large diameter. The weight and capacity change synchronously with the change of diameter and length. When all-metal vessels are placed into a container, their total capacity can exceed the total capacity of metal plastic

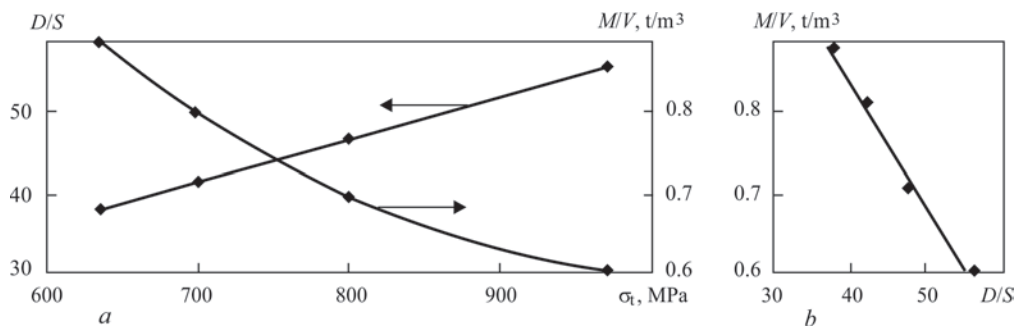


**Figure 1.** Effect of  $\sigma_t$  of pipe steel on  $D/S$  and  $M/V$  (a) and  $D/S$  on  $M/V$  (b) of all-metal vessels of 351–610 mm diameter

vessels, due to absence of the fiberglass casing. The volume of gas in the container is almost independent on the diameter of vessels placed into it.

$M/V$  characteristic is practically independent on the vessel diameter and length, when keeping  $l_c/D = 5-7$  and higher.

$$M/V = \rho \left[ 2 \frac{K_s p}{\sigma_t} + \left( \frac{K_s p}{\sigma_t} \right)^2 \right]$$

is determined by steel strength, coefficient of safety of the vessel and gas pressure ( $\rho = 7.85 \text{ t/m}^3$  is the steel density). Practical independence of  $M/V$  from dimensional parameters of the vessel allows quick assessment of this characteristic, before designing the vessel.

Multipass arc welding from one side of roll-welded butt joints of pipes and bottoms with the wall thickness of 9.0–13.2 mm with U-shaped groove, allowing for [9, 18–20], is conducted with performance of gravity welding of the root pass by consumable electrode gas-shielded arc process, in particular, using  $\text{CO}_2$ ; nonconsumable electrode argonarc welding and coated electrode welding. Small weight of the weld pool in tungsten electrode argonarc welding with activating flux and metal solidification from the side walls (Figure 2), promote prevention of molten metal flowing out and improve formation of the welded joint from the reverse side. Subsequent filling of the groove can be continued by the above-mentioned welding processes. Circumferential joints are subjected to local tempering, in particular with flexible electric heaters.

Multilayer weld metal of experimental butt joints of X80 steel, made by submerged-arc welding, has ferrit-



**Figure 2.** Primary microstructure of metal ( $\times 50$ ) of root and subsequent layers of the weld of butt joint

ic-bainitic structure with MAK-phase inclusions (Figure 3), similar to metal of the longitudinal weld of prefabricated pipes [21]. Its higher hardness of  $HRB 88-91$ , compared to  $HRB 72-75$  and  $71-72$  of the base metal and HAZ is practically preserved after high-temperature tempering ( $HRB 88-89, 71-73$  and  $70-73$ ).

Microstructure of metal of welded joint on 30KhGSA steel is a mixture of martensite, bainite, as well as ferrite (Figure 4) [22]. In the points of repeated short-time heating below the start of austenitic transformation  $A_{c1}$ , there is a tendency to formation of the structure of tempered sorbite. In the upper part of the joint made by nonconsumable electrode argonarc welding, the metal of the weld and HAZ regions adjacent to it has high hardness  $HV0.2-390-500$ , which decreases to  $HV0.2-230$ , when removed from the weld towards the thermally improved base metal with hardness  $HV0.2-280-300$  (Figure 5, a). Metal in the weld lower part has lower hardness  $HV0.2-260-300$ , due to tempering at heating during welding. Longer

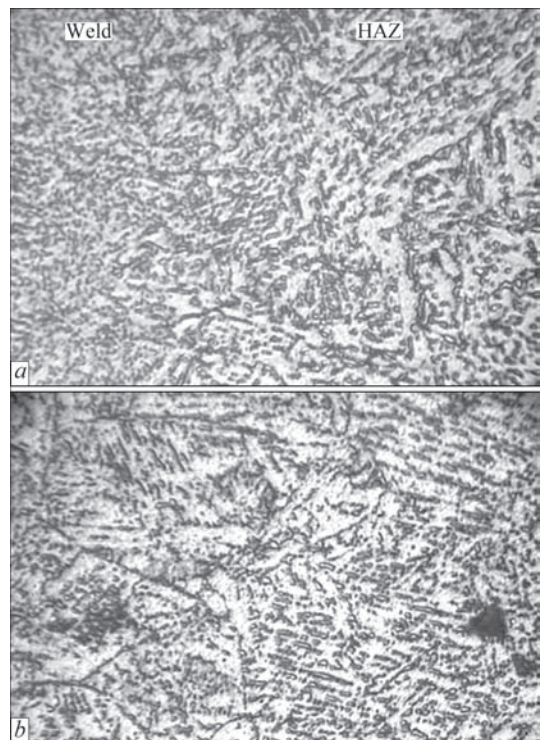


**Figure 3.** Microstructure ( $\times 320$ ) of metal of fusion zone (a) and HAZ (b) of steel of X80 grade

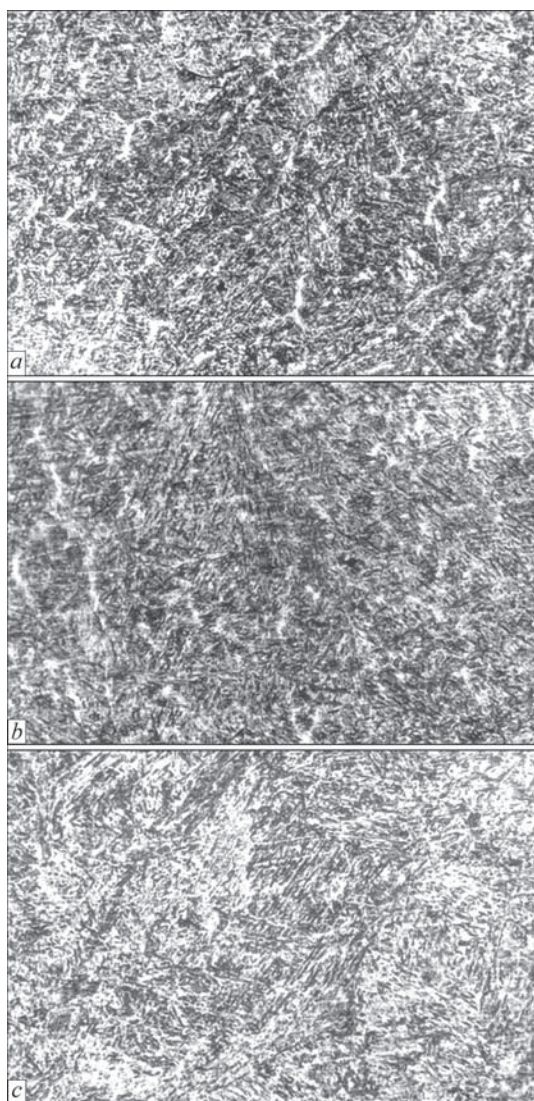


**Figure 4.** Microstructure ( $\times 320$ ) of metal of root (*a*) and subsequent (*b*) layers of weld and fusion zone (*c*) of 30KhGSA steel

postweld local tempering leads to lowering of metal hardness in the weld upper and lower parts to  $HV_{0.2}$ –330–420 and  $HV_{0.2}$ –230–240 (Figure 5, *b*). In highly tempered welded joint made with Np-30KhGSA wire in  $CO_2$ , a distribution of hardness  $HV_{0.2}$ –270–330, which is uniform in width and height, is achieved.

Impact toughness  $KCU_{20}$  in weld metal of 10Kh2M type and HAZ of test butt welded joints of X80 steel rises slightly from 86 to 87–95 and from 286 to 289–305 J/cm<sup>2</sup> at performance of high-temperature tempering, respectively. Microalloyed manganous weld metal of pipes for the main pipelines has higher value of  $KCV_{20} = 110$ –120 J/cm<sup>2</sup> [21]. In highly tempered weld metal of 18KhM type in 30KhGSA steel this value is  $KCU_{20} = 90.9$  J/cm<sup>2</sup>. The given impact toughness values of welded joints exceed minimum admissible values of  $KCU_{20} = 50$  J/cm<sup>2</sup> and  $KCV_{20} = 35$  J/cm<sup>2</sup> [14].

Higher strength of weld metal leads to statically tested welded samples failing beyond the weld. Higher strength metal is characterized by higher fa-

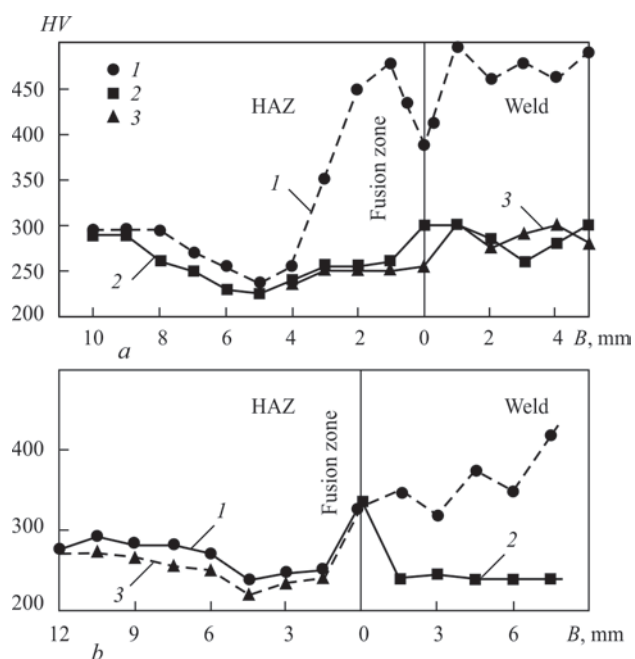


**Figure 5.** Distribution of microhardness in the upper (*1*), lower (*2*) and middle (*3*) part of a butt joint of heat-treated 30KhGSA steel 10 mm thick after argonarc welding (*a*) and subsequent local tempering (*b*)

tigue resistance. Cyclic fatigue life at tension up to  $\sigma_1 = 350$  MPa of flat welded samples from X80 steel in the straightened part of a large diameter pipe after submerged-arc butt welding is 86100 cycles to fracture from the point of transition of a weld with approximately 1.5 mm height of reinforcement to the base metal. It rises to 114100 cycles after high-temperature tempering, and at combination of high-temperature tempering with smaller load  $\sigma_1 = 300$  MPa, it increases to 312400 cycles. Established number of cycles of uniaxial tension to fracture of samples from X80 steel, welded by submerged-arc process, is higher than 5200–7800 cycles of gas filling and discharge 2–3 times per week for 50 years of operation by 11–22 times and more. It is much higher than 15000–24000 cycles of hydraulically tested combined car bottles with heat-strengthened and fiberglass-reinforced body from alloyed steel [23].

With lowering of weld reinforcement height to 0.3–0.5 mm and improvement of welded joint formation at nonconsumable electrode argonarc welding of 30KhGSA steel, the cyclic fatigue life of samples in as-welded and locally as-tempered condition is higher than 217800 and 229200 loading cycles at  $\sigma_1 = 350$  MPa (fracture along the fillet). After reduction of fillet roughness the welded samples do not fail during 584400 and 674400 cycles at the same load, exceeding  $\sigma_w^m = 192$ –194 and 267 MPa, equal to  $0.273$ – $0.278\sigma_t$  of non-heat treated and heat-treated steel of seamless pipes. Fatigue limits  $\sigma_{-1}$  of about  $0.4\sigma_t$  of steel [24] and  $\sigma_0 = 0.27$ – $0.30\sigma_t$  of welded

joints of low-alloyed high-strength steels [25] are higher than  $\sigma_w^m$ , and there is no risk of fatigue fracture of circumferential joints, because of varying gas pressure in the all-metal vessel.

## Conclusions

1. The rationality of simplified manufacture of welded high-pressure vessels for delivery of natural gas and supplying gas to small companies is substantiated. This is achieved by application of prefabricated pipes of medium diameter from higher strength steels (X80, 30KhGSA, X100) and elimination of high power-consuming operations for forming the outer fiberglass casing and manufacture of heat-strengthened welded shell from the technological process. Less strong low-alloyed (and carbon high-quality) sheet structural steels are acceptable for manufacture of bottoms of all-metal vessels.

2. Relatively small wall thickness, diameter and weight of the vessels enable simplification of performance of welding and rigging operations, reducing the number of passes and welding time, welding material and power consumption. Performed circumferential joints of all-metal vessels do not fail at constant and changing gas pressure.

3.  $M/V$  ratio of all-metal vessels depends little on vessel dimensions. This characteristic is operatively assessed by the strength of pipe steel without  $M$  and  $V$  determination.

4. Free access to the cylindrical surface of the vessel promotes simplification of maintenance and repair-reconditioning operations performance. Manufacture of all-metal vessels with application of medium diameter pipes requires simple welding equipment. Its organization does not raise any special difficulties.

*The author is grateful to V.P. Elagin and A.Z. Kuzmenko for assistance in studying the hardness distribution and low-cycle fatigue of welded joints.*

1. Paton, B.E., Savitsky, M.M., Savitsky, A.M. et al. (2014) Effectiveness of natural gas transportation by sea at application of high pressure welded cylinders. *The Paton Welding J.*, **8**, 47–53.
2. Blinkov, A.N., Vlasov, A.A. (2006) Compressed gas transportation by sea. New possibilities for field development of natural gas in shelf. *Morskaya Birzha*, **2**, 65–69 [in Russian].
3. Blinkov, A.N., Vlasov, A.A., Latsis, A.V., Shurnyak, V.K. (2007) New technology of gas transportation by sea: State-of-the-art, problems, perspectives. *Sb. Registra Sudokhodstva*, St.-Petersburg, **30**, 127–162 [in Russian].
4. Ren, Ch.G., Zelenskaya, E.V. (2011) Review of existing methods of natural gas transportation for long distances and assessment of their application. *Neft, Gaz i Biznes*, **3**, 3–9 [in Russian].
5. Zajtsev, Val. V., Zajtsev, V.A., Kotova, E.V., Skripnichenko, K.S. (2010) Analysis of specifics of requirements of classification societies to ships transporting compressed natural gas. *Zb. Nauk. Prats NUK*, Mykolaiv, 5(434), 11–18 [in Russian].

6. Savitsky, M.M., Savitsky, A.M., Suprunenko, V.A. et al. (2013) Determination of parameters of light-weight welded cylinders for cargo system of CNG carriers. *Elektronny Vestnik NUK*, **1**, 4–11 [in Russian].
7. Savitsky, M.M., Kulyk, V.M., Lupan, A.P. et al. (2008) *Method of manufacture of composite cylinder*. Pat. 83095 Ukraine [in Ukrainian].
8. Kulyk, V.M., Savitsky, M.M., Elagin, V.P., Demchenko, E.L. (2012) *Method of manufacture of composite vessel*. Pat. 100273 Ukraine [in Ukrainian].
9. Kulik, V.M., Savitsky, M.M., Elagin, V.P., Demchenko, E.L. (2011) Capabilities of application of high-strength low-alloy pipe steels for manufacture of high-pressure vessels. *The Paton Welding J.*, **2**, 43–47.
10. Kulyk, V.M., Savitsky, M.M., Suprunenko, V.O. (2016) *Combined cylinder*. Pat. 11268 Ukraine [in Ukrainian].
11. Tukhbatullin, F.B., Galiullin, Z.T., Karpov, S.V. et al. (2001) Low-alloy steels for main gas pipelines and their resistance to fracture. *Inform. Rev. Ser. Transport and overhead storage of gases*. Moscow, IRTs Gazprom [in Russian].
12. Bayer, D., Flus, P., Amoris, E. et al. (2006) Microstructure and characteristics of pipe steels after thermal and mechanical treatment. *Novosti Chyorn. Metallurgii za Rubezhom*, **4**, 65–76 [in Russian].
13. Nabuki, I., Shigeri, E., Jos, K. (2006) UOE pipes with high characteristics for main pipelines. *Ibid.*, 77–80 [in Russian].
14. (1998) *Regulations of design and safe operation of pressure vessels*. Kiev [in Ukrainian].
15. Pisarenko, G.S., Agarev, V.A., Kvitka, A.L. et al. (1967) *Strength of materials*. Ed. by G.S. Pisarenko. Kiev, GITL Ukr. SSR [in Russian].
16. (2008) *STO Gazprom 2-2.3-184-2007*: Procedure on calculation and substantiation of safety and stability factors of main gas pipelines at the stage of service and maintenance. Moscow [in Russian].
17. Paton, B.E., Savitsky, M.M., Savichenko, A.A., Suprunenko, V.A. (2009) High-pressure vessels for natural gas. In: *Problems of welding, related processes and technologies*. Nikolaev, 89–90 [in Russian].
18. Kakhovsky, N.I., Fartushny, V.G., Yushchenko, K.A. (1975) *Electric arc welding of steels*: Refer. Book. Kiev, Naukova Dumka [in Russian].
19. Kulyk, V.M., Savitsky, M.M., Lupan, A.P., Chertorylsky, L.O. (2007) *Method of multipass nonconsumable electrode welding*. Pat. 81953 Ukraine [in Ukrainian].
20. Kulik, V.M., Savitsky, M.M., Lupan, A.F. et al. (2007) Argonarc welding of billets of shafts for metallurgical equipment. *The Paton Welding J.*, **10**, 28–32.
21. Rybakov, A.A., Filipchuk, T.N., Kostin, V.A. (2015) Peculiarities of microstructure and impact toughness of metal of welded joints of pipes of high-strength steel with niobium and molybdenum. *Ibid.*, **3-4**, 16–23.
22. Kulik, V.M., Vasiliev, V.G., Grigorenko, G.M. et al. (2007) Phase and structural transformations in welding and arc treatment of 30KhGSA steel joints. *Ibid.*, **9**, 6–10.
23. Savitsky, M.M., Savichenko, A.A., Kulik, V.M. et al. (2007) Light-weight welded cylinders for motor transport. *Ibid.*, **1**, 43.
24. Serensen, S.V., Shnejderovich, R.M., Gusenkov, A.P. et al. (1975) *Strength under low-cycle loading*. Moscow, Nauka [in Russian].
25. Trufyakov, V.I. (1973) *Fatigue of welded joints*. Kiev, Naukova Dumka [in Russian].

Received 08.02.2018

## POSSIBILITIES OF MANUFACTURING THREE-LAYER WELDED HONEYCOMB PANELS FROM ALUMINIUM ALLOYS

L.V. PETRUSHINETS, Yu.V. FALCHENKO, V.E. FEDORCHUK and V.S. SHINKARENKO

E.O. Paton Electric Welding Institute of the NAS of Ukraine  
11 Kazimir Malevich Str., 03150, Kyiv, Ukraine. E-mail: [office@paton.kiev.ua](mailto:office@paton.kiev.ua)

Three-layer honeycomb panels are widely applied in aircraft construction, ship-building, construction and others industries. In terms of design, they consist of a honeycomb core and two skins. At relatively small weight, these structures are characterized by high strength values, sound- and heat-insulating properties. The main problem in manufacturing a three-layer structure is welding the upper and lower skins to end faces of the honeycomb core. The work presents the results of development of the technology of manufacturing three-layer honeycomb panels of 150×150 mm size from aluminium alloys. The honeycomb core from AD1 aluminium alloy 0.150 mm thick was produced by joining the corrugated strips into blocks by spot welding. Flatness of end faces of the honeycomb core was achieved by grinding. The structure rigidity was ensured by filling the cells with colophony. Joining of the core to the skins from AMg2 alloy 1.0 mm thick was performed by diffusion welding in vacuum. The process was conducted in a fixture consisting of the lower and upper flanges and bushing. The flanges provided skin pressing to the honeycomb core end faces over the entire contact area, and the bushing allowed homogenizing the temperature field in the item and controlling the extent of its deformation during welding. 8 Ref., 1 Table, 6 Figures.

**Keywords:** *three-layer honeycomb panel, sheet aluminium alloys, spot welding, diffusion welding in vacuum*

Three-layer panels are widely applied at present in aircraft construction, ship-building and other industries. At a relatively small weight these structures have high characteristics of strength and rigidity. Load-carrying layers, reinforced by the core, take high compressive stresses, exceeding the material limit of elasticity. This kind of structures is characterized by good vibrational, radio engineering, sound and heat-insulating properties [1, 2].

A number of methods are used for joining the honeycomb core elements: adhesive bonding, resistance welding, brazing and diffusion welding. The most widely accepted manufacturing method is adhesive bonding (about 95 %). Three-layer honeycomb panels from aluminium alloys are mostly produced by adhesive bonding in modern industry. Panels produced by brazing, resistance and diffusion welding, are applied in structures, operating at high temperatures or in aggressive media [1]. Accordingly, nichrome, titanium alloys or stainless steels, are the materials used for such panels.

Honeycomb cores are produced by one of the two methods: pack stretching or its manufacture from profiled strips. With the second method, welding or brazing can also be applied, alongside adhesive bonding. The pack stretching method is used for manufacturing

the cores, in which the honeycombs consist of just six faces. Here the thicknesses of metallic materials do not exceed 80  $\mu\text{m}$ . The honeycomb cores, made from profiled strip in the form of foil, have more regular honeycomb geometry, that the cores produced by pack stretching. This technological process takes more time than the method of pack stretching. Therefore, the cores produced from profiled strips are usually more expensive [1].

The three-layer panel is designed to consist from two skins and honeycomb core, which differ essentially, both in their geometry and mechanical properties in different planes. This kind of structure requires development of individual approaches both to welding of profiled strips into the honeycomb core block, and to formation of the tee-joint of the skins with the core.

The objective of this work was development of the technology of producing three-layer honeycomb panels from aluminium alloys by diffusion welding in vacuum.

Three-layer panels were manufactured with application of AD1 aluminium alloy with foil thickness of 0.15 mm for the core, and AMg2 alloy of 1.0 mm thickness for the skins.

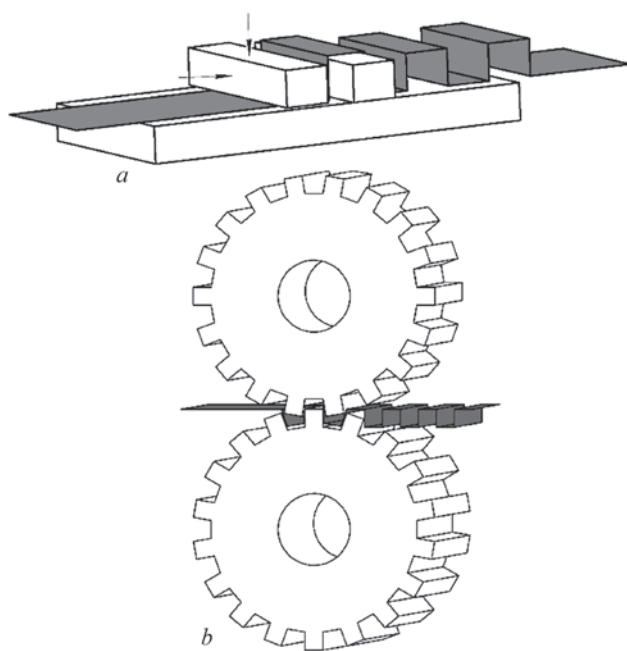


**Figure 1.** Schematic of moulding the honeycomb core strips using rectangular inserts (a) or a gear set (b)

Based on the earlier performed literature survey [3], it was shown that profiled strips for the honeycomb core can be produced by successive moulding of foil with the specified step in the form of halves of honeycombs in the fixture consisting of rectangular inserts (Figure 1, a) or using a gear set (Figure 1, b).

The first type of fixture is simple to manufacture, but forming the profiled strips takes considerable time. The fixture, consisting of a gear set, is more expensive to manufacture, but it is rational when preparing large batches of profiled strip.

Spot and diffusion welding methods were applied to join the elements of profiled strips into the honeycomb core block. Spot welding was conducted on a support strap made from steel in the form of a «comb» (Figure 2). Fixture, consisting of a set of «combs» was used for diffusion welding, respectively.

Mechanical tensile tests of welded joints of foil were performed in versatile MTS 810 machine. Mechanical compression characteristics of the honey-

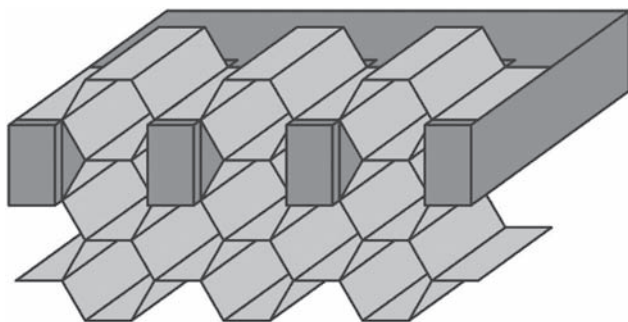


**Figure 2.** Appearance of «comb» fixture for welding the honeycomb core

#### Tensile strength of joints

Sample	Welding mode			Fracture site	$\sigma$ , MPa	$\sigma_{av}$ , MPa
	$T_w$ , °C	$P_w$ , MPa	$t_w$ , min			
BM	-	-	-	-	67.9	68.0
				-	58.9	
				-	77.3	
Welded joint	600	40	20	Grips	59.7	64.0
				Same	56.1	
				Joint zone	76.1	

comb structure were studied with application of digital controller of KOLI Company, XK3138T1 model, and pressure sensor of CAS Company, MNC-1 model, with operating range from 0 up to 1000 kg.

Vacuum diffusion welding was performed in P-115 system by the procedure, described in detail in [4].

Investigation of welded joint microstructure was conducted on transverse microsections, using scanning electron microscope, fitted with energy-dispersive spectrometer ENERGY 200 and optical metallographic microscope MMT-1600V.

Vacuum diffusion welding of AD1 aluminium alloy was performed at temperature  $T_w = 480\text{--}600$  °C, pressure  $P_w = 10\text{--}40$  MPa, process duration  $t_w = 10\text{--}20$  min, vacuum in the chamber was maintained on the level of  $1.33 \cdot 10^{-3}$  Pa. Oxide film was removed by mechanical scraping, which was followed by degreased the surfaces to be welded in alcohol. The size of overlapping of the samples to be welded was 10 mm.

As shown by investigations, in foil welding in the mode, which corresponds to the optimal one according to published data [5], individual adhesion areas are observed in the sample joint zone. It is found that pressure increase up to 40 MPa and process duration of up to 20 min provided physical contact over the entire surface of the sample. At increase of welding temperature from 480 up to 600 °C the quantity of defects in the joint zone is reduced.

Mechanical tensile properties were determined both for aluminium foil in the initial condition, and for welded joints (see Table). It is found that strength of initial metal from AD1 alloy is equal to  $\sigma_t = 68.0$  MPa. Average strength of welded samples is equal to  $\sigma_t = 64.0$  MPa, i.e. coefficient of joint strength is equal to 0.94 of the initial material level.

Spot welding was performed at room temperature in air. Before welding, the foil contact surfaces were mechanically scraped and degreased. The process was conducted in the following modes:  $U_w = 3$  V, current  $I_w = 270\text{--}300$  A. The intensity of heating in welding was determined by process duration, which was set by time switch in the range of  $t_w = 0.2\text{--}5.0$  s. Visual in-

spection of the surface and tensile testing of the joints showed that the optimum duration of the welding cycle is  $t_w = 0.5\text{--}1.0$  s.

In samples produced at less than 0.5 s pulse duration, partial melting of the joined surfaces under the electrode is observed with formation of weld spots of a small diameter (Figure 3, *a*). Increase of welding time up to 1 s allows improving the welding quality and promotes formation of a tight joint over the entire electrode surface (Figure 3, *b*).

Considering that the diffusion welding process is more labour-consuming, further on spot welding was used for welding the honeycomb core elements.

Resistance of the honeycomb core to the impact of external loads was determined by compression tests, in keeping with the procedures given in studies [6, 7]. It is found that deformation of the honeycomb core from AD1 alloy occurs at the average value of the compressive force equal to 23.3 MPa. Analysis of honeycomb core elements after compressive testing showed that no delamination of the walls occurs during deformation.

During manufacture of the three-layer panel it is necessary to join the honeycomb core to the skins, thus ensuring formation of tee-joints. Diffusion welding in vacuum is the most suitable for these purposes, as it allows maximum accurate control of all the process parameters.

One of the main requirements in diffusion welding is the plane-parallelism of the surfaces being welded. However, the technology of producing the honeycomb core from profiled strips does not ensure it. Stresses arising during spot welding, result in distortion of the honeycomb core block. Therefore, we developed the technology of grinding its contact surfaces. Considering that the honeycomb core is made of an aluminium alloy 0.15 mm thick, its direct machining is impossible in view of its high ductility. To provide the stability of the cell walls, it is necessary to ensure their rigidity by filling them with another material. The material for honeycomb filling should meet the following requirements:

- have low melting temperature;
- be sufficiently rigid and strong;
- be inert to the material of honeycomb core — aluminium;
- be readily treatable by grinding;
- be easy to remove.

Applicability of colophony, sulphur and paraffin as material for filling the honeycomb core was studied.

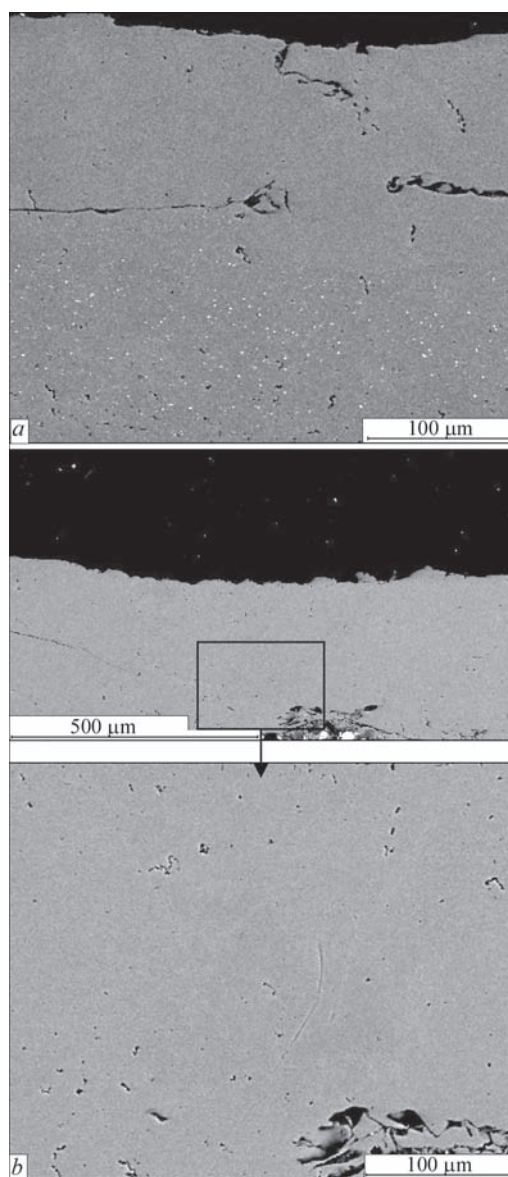


**Figure 3.** Microstructure of joints produced by spot welding at process duration of 0.2 (*a*) and 1 s (*b*)

When sulphur is used ( $T_m = 115$  °C), one should take into account that it has a higher viscosity above 160 °C, that makes it unsuitable for application. Sulphur melt acquires the highest viscosity at the temperature of 190 °C. Further temperature rise is accompanied by lowering of viscosity and above 300 °C the fluidity of molten sulphur increases again. Therefore, cell filling should be performed at the temperature of 300–350 °C.

Paraffin has melting temperature  $T_m = 45\text{--}65$  °C, but shows considerable shrinkage at solidification, so that filling has to be conducted in several stages.

Colophony melts at temperature  $T_m = 100\text{--}130$  °C. It has a sufficiently low viscosity in the molten state that has a positive effect on adaptability to fabrication (fillability of the form). Moreover, shrinkage of colophony at solidification is minimal.

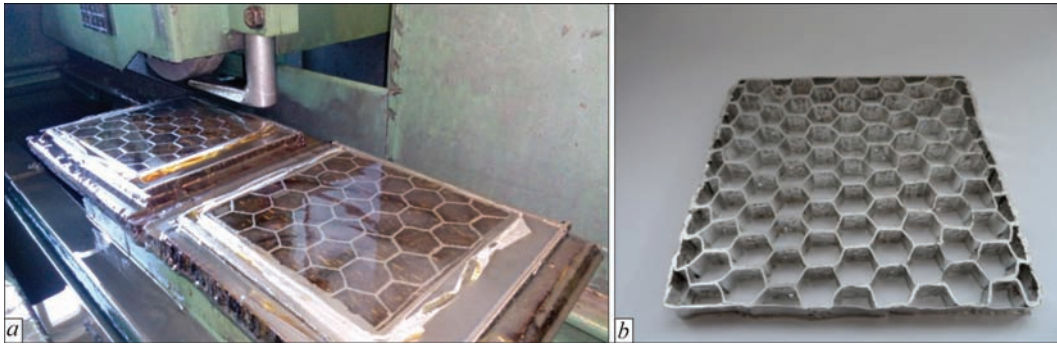


**Figure 4.** Appearance of honeycomb core during grinding (a) and after removal of colophony (b)

Honeycomb core samples were filled with the respective substance (colophony, sulphur, paraffin) in the molten state, and left to solidify for 20–30 min, which was followed by grinding of the contact surfaces (Figure 4, a).

As followed by the conducted experiments, the samples filled with colophony, have the best grindability. When paraffin is used, it sticks to the abrasive tool, making the grinding process more difficult. At application of sulphur, some surface areas, where it has delaminated, are observed, that leads to deformation of the core walls.

Technological operation of removing the material poured into the honeycomb core cells was conducted using sample reheating. Experiments showed that paraffin remains are readily removed from the cells, if final rinsing is performed in boiling water. In samples filled with sulphur, a small deposit remains on cell surface after its removal, which is difficult to remove after washing in benzene. In the case of colophony application, its remains are readily removed by washing in organic solvents: alcohol, benzene and turpentine.

Performed research leads to the conclusion that it is the most rational to apply colophony as material for filling the honeycomb core cells. It allows performing high-quality machining and subsequent scraping of all the faces of honeycomb cells (Figure 4, b).

Diffusion welding of three-layer honeycomb panel of 150×150 mm size was conducted in a special-

ized device, which is designed to consist of the lower and upper flanges and limiting bushing (Figure 5, a). Flanges ensure pressing of the skins to the honeycomb core over the entire contact area during welding. The purpose of the limiting bushing consists in equalizing the temperature field and ensuring the specified level of overall plastic deformation on the item [8]. The welding mode corresponded to the following parameters:  $T_w = 540\text{ }^\circ\text{C}$ ,  $P_w = 5\text{ MPa}$ ,  $t_w = 20\text{ min}$ . Figure 5, b shows the appearance of the three-layer honeycomb panel manufactured by the developed procedure.

As shown by the results of optical microscopy, there are no defects in the form of cracks or pores in the zone of the joint of honeycomb core wall and the skin (Figure 6, a).

Compressive testing of the three-layer panel elements was performed to assess the strength of their joining. For this purpose, individual elements corresponding to an isolated hexagonal cell by their dimensions were cut out of the three-layer panel.

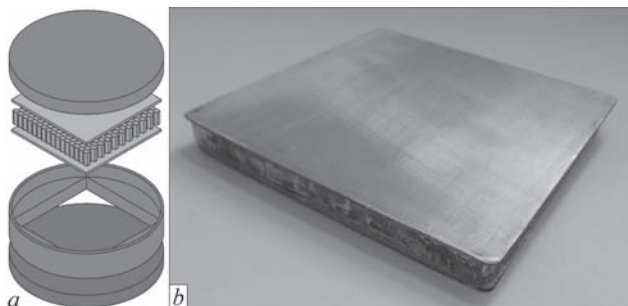


**Figure 5.** Schematic of the fixture with panel elements (a) and appearance of three-layer honeycomb panel after welding (c)

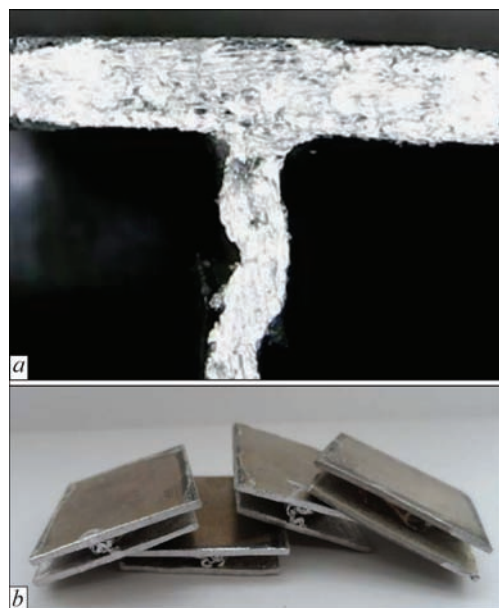


**Figure 6.** Macrosection of a tee-joint of the wall of honeycomb core and the panel skin (a) and appearance of samples cut out of the three-layer panel after their compressive testing (b)

The dimension of the honeycomb core cells was 10×10 mm, its height was 11 mm, thickness of AMg2 aluminium alloy skins was 1 mm, and thickness of honeycomb core from AD1 alloy was 0.15 mm. Total area of the sample surface was about 670 mm<sup>2</sup>, and the cross-sectional area of the honeycomb core was 12 mm<sup>2</sup>.

As is seen from Figure 6, *b*, at compression with the degree of deformation of about 50 %, deformation of vertical walls of the core proceeds without fracture of the sections of welding the honeycomb core to the panel skins. Average value of compressive force, at which deformation of the honeycomb core in the three-layer panels takes place, is equal to 58.12 MPa.

Thus, performed investigations showed the theoretical possibility of manufacturing welded three-layer panels from aluminium alloys. Developed technology of grinding the honeycomb core enabled producing the joint over all the contact surfaces of the three-layer panel. Analysis of mechanical testing results showed that the panels with the honeycomb core in the form of hexagonal cells can stand compressive

loading with the degree of deformation of the order of 50 % without fracture of tee welded joints.

1. Bitzer, T. (1997) *Honeycomb technology: Materials, design, manufacturing, applications and testing*. Springer-Science+Business Media Dordrecht.
2. Panin, V.F., Gladkov, Yu.A. (1991) *Structures with filler: Refer. book*. Moscow, Mashinostroenie [in Russian].
3. Falchenko, Yu.V., Petrushinets, L.V. (2018) Modern methods of manufacturing three-layer panels of aluminium alloys (Review). *The Paton Welding J.*, **6**, 38–46.
4. Ustinov, A.I., Falchenko, Yu.V., Melnichenko, T.V. et al. (2013) Diffusion welding of aluminium alloy strengthened by Al<sub>2</sub>O<sub>3</sub> particles through an Al/Cu multilayer foil. *J. Materials Proc. Technology*, **213**, 543–552.
5. Kozakov, N.F. (1968) *Vacuum diffusion welding*. Moscow, Mashinostroenie [in Russian].
6. Heimbs, S., Schmeer, S., Middendorf, P., Maier, M. (2007) Strain rate effects in phenolic composites and phenolic-impregnated honeycomb structures. *Composites Sci. and Technology*, **67**, 2827–2837.
7. Xu, S., Beynon, J.H., Ruan, D., Lu, G. (2012) Experimental study of the out-of-plane dynamic compression of hexagonal honeycombs. *Composite Structures*, **94**, 2326–2336.
8. Falchenko, Yu.V., Ustinov, A.I., Petrushinets, L.V. et al. (2017) *Device for diffusion welding of three-layer honeycomb panels*. Pat. 113424, Ukraine, Int. Cl. B23K 20/00, B23K 20/14.

Received 04.06.2018

# CALCULATION OF PENETRATION ZONE DIMENSIONS IN SURFACING OF ROLLS FOR BILLET CONTINUOUS CASTING MACHINES

V.N. MATVIENKO, L.K. LESHCHINSKY and V.A. MAZUR

State Higher Education Institute Pryazovsky State Technical University  
7 Universitetskaya Str., 87500, Mariupol, Ukraine. E-mail: [matviyenko@gmail.com](mailto:matviyenko@gmail.com)

It is shown that in surfacing rolls of billet continuous casting machines (BCCM) the dimensions of the penetration zone are affected by chemical composition and thermophysical properties of the material of the roll or deposited sublayer. The calculated values of the cross-sectional area, penetration depth and volume of molten metal are presented. They were obtained by numerical modeling on the basis of solving the nonlinear three-dimensional differential equation of thermal conductivity, taking into account the approximated temperature dependence of thermal conductivity coefficient. It was established by calculation and confirmed by experiment that the dimensions of penetration zone increase at submerged-arc surfacing with strip electrode of a sublayer of martensitic-ferritic high-chromium steel and to a higher extent at surfacing of a sublayer of chromium-nickel steel as compared to surfacing of the roll material or of a sublayer of low-carbon low-alloyed steel. 10 Ref., 3 Tables, 3 Figures.

**Keywords:** *roll of a billet continuous casting machine, base metal, submerged-arc surfacing, strip electrode, penetration zone, dimensions, numerical modeling, deposited layer, sublayer, chemical composition, thermophysical characteristics, thermal conductivity coefficient*

In manufacture and reconditioning of the rolls of billet continuous casting machines (BCCM) the longitudinal bending of the roll can be reduced, and the probability of defect initiation can be lowered by reducing the volume of deposited metal by limiting the number of deposited layers [1, 2]. In the case of application of surfacing with two layers, namely sublayer (intermediate layer) and outer layer [3], the required content of alloying elements in the outer layer depends both on electrode composition, and on the degree of outer layer dilution by the sublayer, and when surfacing through the sublayer it depends on roll material. Even small changes of the degree of dilution can lead to noticeable deviations in the content of alloying elements in the outer layer. Such deviations from the composition of Kh13 type (in particular, 08Kh13N3M1AFB, widely applied for surfacing the outer layer of BCCM rolls) lead to lowering of the resistance to corrosion-mechanical wear, thermal cycles, and thermal fatigue fracture [4, 5]. Here, the possibility of producing the composition of Kh13 type in the outer layer depends not only on substantiation of selection of materials and surfacing mode parameters, but also on the dimensions of the penetration zone, that leads to increase of the requirements to the accuracy of prediction of its dimensions.

**Initial data for calculation of penetration zone dimensions.** Selection of initial data for calculation was performed, proceeding from preliminary analysis of the composition and thermophysical properties of

both the base material of BCCM rolls, and composition of metal for deposition of the sublayer and outer layer. From materials used for roll manufacture, we should single out heat-resistant steel 25Kh1M1F of pearlitic class, steel 25Cr1Mo1V of close composition, as well as steel 42CrMo4 with higher content of carbon and lower content of chromium and molybdenum [3–5]. Application of low-carbon low-alloyed steels 06KhN2G1M, 10Kh1M1G1N, 10GS, 12Kh1MF ensures producing a ductile sublayer [2]. At two-layer surfacing the sublayer composition with a higher (than that in the outer layer) content of chromium, for instance, of Kh17 type, as well as other alloying elements, primarily, nickel and molybdenum, can be chosen [3]. Steels 08Kh17N12M2, 0Kh18N10, 0Kh19N11M3 can be regarded as sublayer compositions with such a content of chromium, which, at the same time, provide an austenitic structure with a high ductility. Unlike the above-mentioned materials, used for manufacturing BCCM rolls and sublayer deposition, the thermophysical properties of which are similar, the properties of austenitic steels, also used for the sublayer, differ considerably. Proceeding from that, calculation of penetration zone dimensions and subsequent analysis were performed for heat-resistant pearlitic steel 25Kh1M1F, martensitic steel 42CrMo4, chromium-nickel austenitic steel 08Kh17N12M2, as well as for high-chromium martensitic-ferritic steel 20Kh13 applied in the sleeves of composite rolls. Chemical composition (Table 1) and structure of the considered steels determine the presented in Table 2

**Table 1.** Chemical composition of steels used in calculations, wt.%

Steel grade	C	Mn	Si	Cr	Ni	Mo	V
25Kh1M1F	0.25	0.6	0.3	1.65	0.25	0.75	0.25
42CrMo4	0.42	0.7	0.4	1.10	0.19	0.20	–
20Kh13	0.20	1.5	1.0	13.0	–	–	–
08Kh17N12M2	0.08	2.0	1.0	17.0	12.0	2.5	(0.4 Ti)

**Table 2.** Physical properties of steels used in calculations (at 20–100 °C) [6, 7]

Steel grade	Coefficient of thermal conductivity $\lambda$ , W/(m·K)	Specific heat, °C, J/(kg·°C)	Coefficient of thermal diffusivity, $a \cdot 10^6$ , m <sup>2</sup> /s	Melting temperature $T_m$ , °C
25Kh1M1F	52	486	12.2	1522
42CrMo4	38	506	7.6	1520
20Kh13	23	452	5.0	1510
08Kh17N12M2	16	468	5.0	1400

thermophysical properties: thermal conductivity coefficient  $\lambda$ , specific heat  $C$ , coefficient of thermal diffusivity  $a$ , melting temperature  $T_m$ . Calculations with application of these data, as well as experimental verification, were conducted for the process of surfacing with strip electrode Sv-12Kh13 of 40 mm thick plates, using AN-26P flux. Mode of RPDC surfacing for 45×0.7 mm strip was as follows: current of 650 A, voltage of 32 V, deposition rate of 12 m/h; for 60×0.5 mm strip — current of 700 A, voltage of 32 V, deposition rate of 10 m/h; strip electrode extension of 40 mm. Surfacing was performed using AD-231 machine and VDU-1202 power source.

**Results of calculation of penetration zone dimensions.** Dimensions of the heating zone, limited by the position of  $T = T_m$  isotherm, were calculated by applying a mathematical model [8, 9], which is based on numerical solution by finite element method of non-linear three-dimensional differential equation of thermal conductivity, which allows for the influence of temperature on thermophysical properties of the base metal. Used for this purpose were equations of continuous functions, characterizing the temperature dependence of the coefficient of thermal conductivity

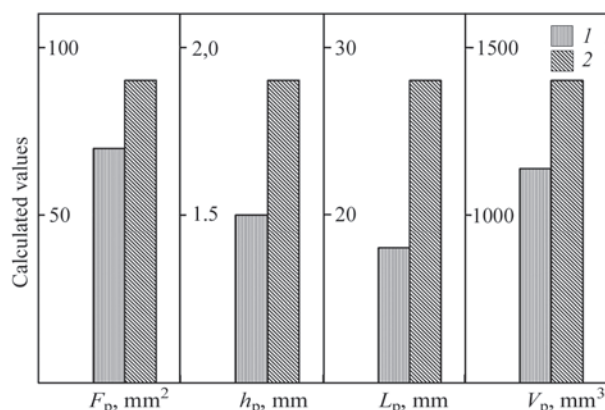
for the considered steels, derived by processing the experimental and calculated data of works [6, 7].

#### Temperature dependence of the coefficient of thermal conductivity

$$\begin{aligned} 25\text{Kh1M1F} & \dots\dots\dots y = -0.0161x + 43.429 \\ 42\text{CrMo4} & \dots\dots\dots y = -0.0127x + 39.424 \\ 20\text{Kh13} & \dots\dots\dots y = 29.113e^{-0.0002x} \\ 08\text{Kh17N12M2} & \dots\dots\dots y = 0.0073x + 13.887 \end{aligned}$$

Calculation results allow assessment of the current values of heating temperature, as well as quantitative characteristics of the thermal field in the zone of base metal melting.

It follows from calculation results (Figure 1) that at unchanged conditions of the process of surfacing with 45×0.7 mm strip electrode, the cross-sectional area, penetration depth and molten metal volume are much smaller for material of the roll from steel 25Kh1M1F, than for a sublayer from steel 08Kh17N12M2. This is confirmed by sections of three-dimensional model of the thermal field of the item in the plane normal to the processed surface, obtained at modeling (Figure 2). Here, it should be noted that as the thermophysical properties of low-carbon low-alloyed steels for sublayer deposition are little different from those of steel 25Kh1M1F, the dimensions of the penetration zone of roll material and such a sublayer also differ only slightly.

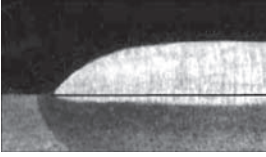
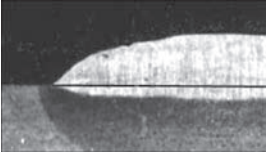


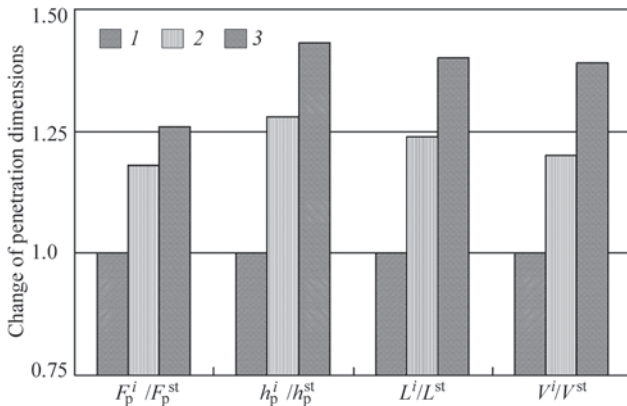
**Figure 1.** Calculated values of penetration zone dimensions (cross-sectional area  $F_p$ , depth  $h_p$ , length  $L_p$ , molten metal volume  $V_p$ ) (45×0.7 mm strip): 1 — deposition on steel 25Kh1M1F; 2 — on sublayer from steel 08Kh17N12M2



**Figure 2.** Boundary of  $T_m$  isotherm in the plane normal to the processed surface (45×0.7 mm strip): a — deposition on steel 25Kh1M1F; b — on sublayer from steel 08Kh17N12M2

**Table 3.** Comparison of calculated and experimental data

Penetration parameters	Roll material steel 25Kh1M1F		Sublayer material steel 08Kh17N12M2	
	Calculation	Experiment	Calculation	Experiment
Area, $F_p$ , cm <sup>2</sup>	68–72	67–73	89–92	88–93
Depth, $h_p$ , mm	1.50–1.55	1.54–1.58	1.90–1.95	1.92–1.98
Transverse macrosection of the deposited bead				

**Figure 3.** Ratio of calculated dimensions of the penetration zone at deposition (60×0.5 mm strip): 1 — on sublayer from steel 42CrMo4; 2 — on steel 20Kh13; 3 — on sublayer from steel 08Kh17N12M2

Influence of substrate metal composition and properties on the ratio of calculated dimensions of the penetration zone is of considerable interest. At surfacing with 60×0.5 mm strip electrode the dimensions of penetration zone on steel 20Kh13 are 1.25 times, and those on steel 08Kh17N12M2 are more than 1.35 times greater than these values for steel 42CrMo4 respectively (Figure 3). Molten metal volume differs to an even greater extent. Comparison of calculated and experimental data on the influence of the composition and properties of steels 25Kh1M1F and 08Kh17N12M2 on penetration area and depth at surfacing with 45×0.7 mm strip electrode (Table 3), confirms the adequacy of the calculation procedure. More precise determination of the geometry of penetration zone by application of the proposed calculation procedure allows substantiation of the change of surfacing mode parameters at development of the technology of reconditioning BCCM rolls. This led to the differentiated approach to selection of the mode, at which the values of heat input in deposition of the surface layer and the sublayer are different, and are determined by their composition and properties [10].

## Conclusions

1. At manufacture and reconditioning of BCCM rolls by surface layer deposition with strip electrode, the penetration zone dimensions depend on chemical composition and thermophysical properties of base metal (roll material), and at deposition on the sublayer they depend on sublayer composition and properties.
2. At deposition on a sublayer from martensitic-ferritic high-chromium steel, and, to a greater extent, on a sublayer from austenitic chrome-nickel steel, the calculated values of cross-sectional area, penetration depth and molten metal volume become higher, compared to deposition on the roll material (pearlitic steel) and on a sublayer from low-carbon low-alloyed steel.

1. Ryabtsev, I.A., Babinets, A.A., Ryabtsev, I.I. (2011) Effect of sub-layer on heat resistance of multilayer deposited metal. *The Paton Welding J.*, **10**, 18–21.
2. Ryabtsev, I.A., Senchenkov, I.K. (2013) *Theory and practice of surfacing operations*. Kiev, Ekotekhnologiya [in Russian].
3. Kirchu, I.F., Stepanova, T.V., Suprun, M.V. (2015) Prospects of application of steel with nitrovanadium hardening for rolls of slab BCCM instead of steel 25Kh1M1F. *Metall i Litio Ukrainy*, **1**, 18–22 [in Russian].
4. Dombrovsky, F.S., Leshchinsky, L.K. (1995) *Operability of surfaced rolls of billet continuous casting machines*. Kiev, PWI [in Russian].
5. (2014) *Cored wires for cladding and thermal metal spraying*. Welding Alloys Group.
6. Mills, K.C. (2002) *Recommended values of thermophysical properties for selected commercial alloys*. England, Cambridge, Woodhead Publishing.
7. Peet, M.J., Hasan, H.S., Bhadeshia, H.K. (2011) Prediction of thermal conductivity of steel. *Int. J. of Heat and Mass*, **54**, 2602–2616.
8. Matvienko, V.N., Mazur, V.A., Leshchinsky, L.K. (2015) Evaluation of shape and sizes of weld pool in surfacing using combined strip electrode. *The Paton Welding J.*, **9**, 28–31.
9. Mazur, V.A., Leshchinsky, L.K., Matvienko, V.N. (2018) Influence of thermophysical properties of base metal on geometry of penetration zone in strip electrode surfacing. *Svarochn. Proizvodstvo*, **3**, 10–14 [in Russian].
10. Matvienko, L.K., Mazur, V.O. (2017) *Method of surfacing of rolls of continuous casting machines*. Pat. 116526, Ukraine, Int. Cl. B23K 9/04 [in Ukrainian].

Received 14.05.2018

# EXPERIMENTAL STUDY OF SLAG AND METAL POOL ROTATION DURING THE ELECTROSLAG PROCESS IN CURRENT-SUPPLYING MOULD

Yu.M. KUSKOV and V.G. SOLOVIOV

E.O. Paton Electric Welding Institute of the NAS of Ukraine  
11 Kazimir Malevich Str., 03150, Kyiv, Ukraine. E-mail: [office@paton.kiev.ua](mailto:office@paton.kiev.ua)

Experiments on studying the rotation of slag and metal pools during the electroslag process in current-supplying mould were conducted. It was found that metal pool rotation can occur both due to the forces of friction from the rotating slag pool, and due to electromagnetic forces applied to the molten metal. Operating current, passing through the mould current-conducting section, has a decisive influence on generation of the rotating effect. 13 Ref., 1 Table, 3 Figures.

**Keywords:** rotation, slag and metal pools, electroslag process, current-supplying mould

The electromagnetic effect on electroslag process showed that under certain conditions it makes possible not only to increase the coefficient of melting of the consumable electrode, but also to change the structure of the solidifying metal [1–3]. At the same time, the basic aim of the most investigations is solving namely the second problem without evaluating the physical phenomena which occur during interaction of the operating current and the magnetic field current.

Actually, the first work, where the process of rotation appearance in a metal pool was studied, was the work [4]. On the basis of the investigations performed on a physical model and evaluation of the results obtained in it, the following conclusion was made: «a metal pool can be brought to rotation only due to the friction forces arising at the contact boundary with a rotating slag pool».

On the other hand, it was shown in works [1, 5, 6] that with the help of external magnetic fields in a metal pool, it is possible to create electro-eddy flows and vibration of the melt as well as its rotation independently of slag movement over its surface due to the action of volumetric electromagnetic forces.

The current-supplying mould (CSM), designed at the E.O. Paton Electric Welding Institute, represents a sectional device, consisting of a nonconsumable circular type electrode, manufactured as a single-turn inductor, and a forming section which is, in fact, a conventional mould [7, 8]. Between these sections an additional intermediate section can be installed, which prevents the liquid metal from getting into the current-carrying section from the forming one.

The electroslag process in the CSM should be accompanied by the same electromagnetic phenomena which occur in the conventional mould using any technology of melting metal, i.e. welding, surfacing, remelting and the action of additional external magnetic field. Nevertheless, the application of CSM, in which its current-carrying section is not an external source of magnetic fields and represents an element of electrical circuit providing the running of the electroslag process with the melting of a remelting metal of any type, supplied into a slag pool, can affect the nature of interaction of the operating current and the magnetic field of the CSM.

This article is devoted to the study of this influence, in particular, on peculiarities of the slag and metal pools rotation.

In a general form, in case of the electroslag process in the CSM, the interaction of the axial component of the magnetic field  $B_z$  (formed by the current-conducting section) with the radial component of the electric current in the slag pool  $I_r$ , should lead to the formation of an azimuthally directed electromagnetic force  $F_\varphi$  rotating the slag around the pool axis.

Moreover, this effect can be pronounced not only in the form of angular displacement of slag layers, but also in the formation of a funnel in the slag at the mould centre. Thus, for example, in edge electroslag surfacing (ESS) in the CSM of 180 mm diameter using a consumable electrode of 40 mm diameter and at a mould current of about 2.4–2.6 kA, the depth of the funnel was more than 50 mm (at a depth of the slag pool of about 110 mm) with its maximum diameter of about 50–70 mm under the electrode end. In connection with such dimensions of the funnel, the electrode

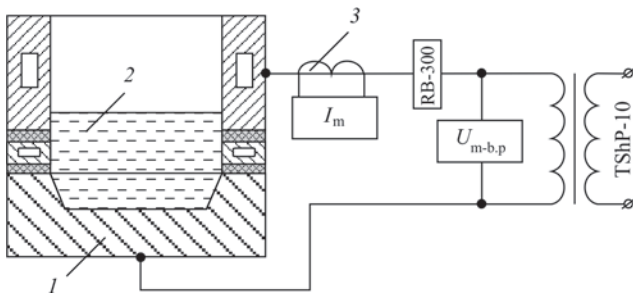


**Figure 1.** Scheme of the physical model for evaluation of slag and metal pool behavior in the CSM: 1 — plug-bottom plate; 2 — mercury; 3 — measuring transformer of current

had to be introduced inside the funnel until its surface came into contact with the slag pool.

A similar situation occurs also in a metal pool. However, the rotational effect is revealed to a much lesser extent, as the components  $B_z$  and  $I_r$  are much lower in the metal pool than those in the slag pool.

The rotational effect is observed when using consumable electrodes, current-free billets, as well as discrete filler both in edge and circular ESS. The determining factor, affecting the slag pool rotation is the current ( $I_{CSM}$ ) passing through the mould current-carrying section.

The Table shows the results of a circular ESS using discrete filler of the 170 mm diameter billet in the broadened CSM of 255/215 mm diameter.

G.V. Ksyondzyk, the designer of the CSM, considered, the same as in work [4], that the rotation of metal pool is transmitted due to friction forces from the rotating slag pool [9].

The comparative melting of a large-section electrode in a conventional mould and of a discrete filler in the CSM showed that in the structure of the metal produced by remelting of the filler, the grain size has about three times smaller dimensions [10]. However, it should be noted that during melting in the CSM it is

Influence of the circular ESS mode on the slag pool rotation speed (flux AN-75)

Surfacing mode		Speed of rotation, rpm
$U, V$	$I_{CSM}, kA$	
28	2.0–2.6	30
40	3.4–3.7	35–40
42	3.6–3.9	36–45
38	3.5–4.0	40–50
32	4.6–4.9	60

difficult to determine what proportion of the influence on these structural changes is due to the inoculating effect of the filler particles, and which one occurs due to the magnetic rotation of the metal pool.

The use of a liquid filler metal (ESS LM) [11, 12] during surfacing allowed showing that even without melt inoculation, the structure of the produced ingots is characterized by a fine-grained structure [13]. However, the authors of the article do not consider the influence of rotation on the structural formation of a solidifying metal. Moreover, the metal produced by ESS LM is compared not with the metal of electroslag melting using consumable electrode, but with the metal melted according to the traditional casting technology. Therefore, the main advantage of the ESS LM metal is associated with a high rate of its solidification.

For a deeper understanding the behavior of slag and metal pools under melting conditions in the CSM, it was decided to carry out experiments on the physical model according to Figure 1. The CSM of 60 mm diameter with the bottom section made in the form of a plug-bottom plate with a groove at its center was filled with mercury of about 40 mm depth. As the source of power the transformer TShP-10 was used. The value of current  $I_m$  was regulated by the ballast resistance RB-300. It was found that during supply of voltage  $U_{m-b,p}$  in the range of 15–30 V from the power source terminals to the current-carrying section of the CSM and the plug, the mercury pool rotation with its little pulsation is occurred.

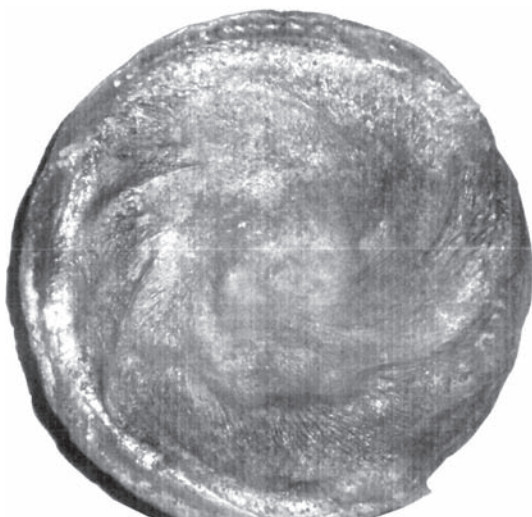


**Figure 2.** Molten surface of the bottom plate primer after a 10-minute electroslag process in the CSM



**Figure 3.** Shape of metal pool in the metal surfaced, formed during electroslag remelting (surfacing) of discrete filler in the CSM

Thus, the interaction of magnetic fields, formed by the operating current passing in the mercury, and the current-carrying section of the mould, contributes to the appearance of a rotational effect in mercury (metal pool) together with the slag pool. The additional data were obtained in a real electroslag process. With this purpose, a slag pool was induced into the CSM of 180 mm diameter on a steel primer of 170 mm diameter and 20 mm thickness, providing a normal operation of the mould and its stable existence at the currents of 2.3–2.5 kA. At the same time, the angular speed of rotation of slag ANF-29 was changed from 72 to 106 rpm during 10 min. After that, the power source TShP-10 was switched off, the slag cap was removed from the mould after its cooling and the primer was inspected. The inspection showed that during the experiment the surface of the primer was fused approximately by 8–10 mm and formed into the shape of a «saucer» with the edges raised approximately by 10 mm around the periphery. From the upper view on the fused surface of the primer (Figure 2), the bands from the rotation of the fused metal are visible and the central part of the primer is little affected by the rotational movement, i.e. the circumferential rotation is observed in practice. Such character of rotation has also influence on the formation of a metal pool of the metal deposited and it can acquire a shape of the «sombbrero» type (Figure 3).

### Conclusions

1. The rotation of metal pool in the CSM can occur both due to the friction forces from the rotating slag pool as well as due to the electromagnetic forces directly affecting the molten metal.

2. The determining effect on the occurrence of rotational effect in the metal pool is provided by the operating current passing through the current-carrying section of the CSM.

3. The centrifugal forces, moving the molten metal to the periphery (walls) of the mould, have a minimum value at its center, which leads to unequal conditions for the formation of a metal pool and its solidification.

1. Trochun, I.P., Chernysh, V.P. (1965) Magnetic control of solidification in electroslag process. *Svarochn. Proizvodstvo*, **11**, 3–5 [in Russian].
2. Topilin, V.V., Klyuev, M.M., Fomicheva, N.P. et al. (1968) Refinement of microstructure of ingots in electroslag remelting of alloys. *Spets. Elektrometallurgiya*, **1**, 23–28 [in Russian].
3. Paton, B.E., Medovar, B.I. (eds) (1986) *Metallurgy of electroslag process*. Kiev, Naukova Dumka [in Russian].
4. Maksimovich, B.I. (1962) Influence of electromagnetic rotation of slag pool on solidification of metal in electroslag remelting of high-alloy steels and alloys. *Elektrotermiya*, **5**, 9–12 [in Russian].
5. Kompan, Ya.Yu., Shcherbinin, E.V. (1989) *Electroslag welding and melting with controlled MGD-processes*. Moscow, Mashinostroenie [in Russian].
6. Protokovilov, I.V., Porokhonko, V.B. (2015) Physical modeling of process of consumable electrode melting in ESR under conditions of external magnetic action. *Sovrem. Elektrometall.*, **1**, 8–12 [in Russian].
7. Ksyondzyk, G.V., Frumin, I.I., Shirin, V.S. (1964) *Current-supplying mould*. USSR author's cert. 264427 [in Russian].
8. Ksyondzyk, G.V., Frumin, I.I., Shirin, V.S. (1969) *Device for electroslag remelting*. USSR author's cert. 337026 [in Russian].
9. Ksyondzyk, G.V. (1975) Current-supplying mould providing rotation of slag pool. *Spets. Elektrometallurgiya*, **27**, 32–40 [in Russian].
10. Kuskov, Yu.M., Skorokhodov, V.N., Ryabtsev, I.A. et al. (2001) *Electroslag surfacing*. Moscow, OOO «Nauka i Tekhnologii» [in Russian].
11. Kuskov, Yu.M. (1996) Electroslag surfacing of cylindrical billets with liquid filler material in current-supplying mould. *Avtomatich. Svarka*, **6**, 52 [in Russian].
12. Medovar, B.I., Chernets, A.V., Medovar, L.B. et al. (1995) Electroslag surfacing with liquid filler metal. *Probl. Spets. Elektrometallurgii* **1**, 6–11 [in Russian].
13. Medovar, B.I., Chernets, A.V., Medovar, L.B. et al. (1997) ESS LM as a method for producing of thin structure of deposited layer from rapid steel. *Ibid.*, **1**, 3–4 [in Russian].

Received 07.05.2018

## INTERNATIONAL CONFERENCE «TITANIUM 2018. PRODUCTION AND APPLICATION IN UKRAINE»

International Conference «Titanium 2018. Production and application in Ukraine» was held on June 11–13, 2018 at E.O. Paton Electric Welding Institute of the NAS of Ukraine (Kyiv). It was organized by the National Academy of Sciences of Ukraine, E.O. Paton Electric Welding Institute of the NAS of Ukraine, JSC «Motor Sich», PJSC «Titanium Institute», Zaporozhye National Technical University, International Association «Welding». The Conference was dedicated to 100 anniversary of the National Academy of Sciences of Ukraine. More than 120 people from 40 organizations participated in it. Among them are the famous scientists of a series of academic institutes of Ukraine, namely academicians L.M. Lobanov, G.M. Grigorenko, O.M. Ivasishin, S.A. Firstov, Z.T. Nazarchuk, corresponding-members S.V. Akhonin and V.M. Nesterenkov, professors of educational institutions, heads and leading specialists of state and commercial enterprises.

Foreign specialists from Physical-Technical Institute of the NAS of Belarus, Polish Institute of Welding, Sichuan Henghui New Material, China, Sichuan Technical Exchange Center, China, Sichuan Vanadium & Titanium Industrial Technology Institute, China, Panzhuhua Innovation and Startup S&T Development, China, Panzhuhua Iron and Steel Group, China, Panzhuhua University, China, ASTEC Engineering GmbH, Austria, Astron Ltd., New Zealand participated in the Conference work.

The Conference was opened by Deputy Director of the E.O. Paton Electric Welding Institute Prof. L.M. Lobanov. He noted relevance of the Conference topics, high importance of the achievements of Ukrainian scientists and specialists in this field, thanked nonresident and foreign participants for their coming and wished all fruitful work.

16 presentations were made at the Conference during plenary session. Presentation of Prof. M.O. Ivasishin from G.V. Kurdyumov Institute for Metal Physics of the NAS of Ukraine «The main tendencies in development of powder metallurgy and titanium 3D technologies» provoked large interest. The main problem of materials science of titanium alloys is de-

velopment of new technological approaches, which would provide decrease of production prime cost of titanium products at retention of unique complex of physicochemical characteristics of these materials. Application of powder technologies in production of titanium alloys and products is an effective method for reduction of their prime cost, increase of competitiveness with other structural materials and, as a result, expanding sphere of practical application of titanium. The presenter told about modern technologies of powder metallurgy of titanium, which provide products with required physicochemical properties being not inferior to properties of the materials received by traditional casting or hot deformation methods. The latest developments in the field of titanium additive manufacturing present the significant interest. They are directed on reduction of production wastes during manufacture of high-quality products for different areas of technique and medicine. Effect of used technological approaches on microstructure, content of impurities, and, as a result, complex of properties of obtained titanium alloys, composites and products of them was discussed in the paper.

Presentation of Prof. S.A. Firstov (I.M. Frantsevich Institute of Problems of Materials Science of the NAS of Ukraine) «Some tendencies in development of new titanium alloys» noted that specific activity in publications dedicated to new titanium-based alloys has two directions, namely high-temperature and heat resistant titanium alloys and titanium alloys of biomedical designation.

Titanium alloys, doped in addition to other «usual» elements (aluminum, tin, zirconium etc.) by boron and silicon as well as intermetallic titanium alloys and titanium alloys strengthened by intermetallics are of interest in the first group.

Based on the affinity of the constitutional diagrams of titanium-silicon and iron-carbon system alloys it is proposed to consider so-called titanium steels and titanium cast irons. Thermomechanical treatment of the first group of alloys containing up to 3 % of silicon allows rising the yield limit to 650 MPa at 700 °C temperature at reaching the strength above 1150 MPa



Presentations of academicians O.M. Ivasishin, S.A. Firstov, corresponding member V.M. Nesterenkov, academician Z.T. Nazarchuk

at room temperature. At that, heat resistance of such alloys significantly exceeds heat resistance of, for example, alloy T16242. In «titanium steels» it is possible in the wide ranges to change the morphology of martensite phases and regulate hardenability varying content of other doping elements.

For «titanium cast irons» it is possible to provide high heat resistance. Yield limit at 800 °C reaches 330 MPa and more. It is possible significantly increasing Young’s modulus to 160 GPa and above. Formation of ternary nanodispersed eutectic structures is of high interest.

In the case with alloys of titanium of biomedical application there is usually a problem of production of alloys with Young’s modulus approaching to Young’s modulus of bone material in order to increase biomechanical compatibility. However, at that reduction of the modulus inevitably involves decrease of strength characteristics.

Therefore, optimizing of strength and elastic characteristics is necessary for specific applications. In order to provide biocompatibility it was proposed to develop the alloys doped with «non-toxic» or even «useful» for human body elements. «Titanium steel» doped with optimum amount of silicon attracts attention in this case the same as with the heat-resistant materials. It is shown that addition of silicon allows dramatically increase biocompatibility of titanium implants in comparison with known alloy VT6 containing «toxic» aluminum and vanadium, and, even, pure titanium.

One of the most important problems is transfer to 3D prototyping that requires solution of the problems



Corresponding Member S.V. Akhonin (in the center) with staff and colleagues

of production of granules with necessary dispersion from new group of alloys.

Presentation of corresponding member of the NAS of Ukraine S.V. Akhonin (E.O. Paton Electric Welding Institute of the NAS of Ukraine) «Development of metallurgy of titanium and alloys on its basis in



Participants from JSC «Motor Sich» during poster session



During the visit to SE SPC «TITAN» of E.O. Paton Electric Welding Institute



At the stand of Zaporozhye Titanium & Magnesium Combine Ukraine» considers the peculiarities of metallurgical production of titanium and titanium semi-finished products in Ukraine.

Titanium is a unique structural material. The alloys based on titanium due to high specific strength have found wide application in aircraft and rocket construction, production of military equipment. Good corrosion resistance of titanium causes its significant application in chemical and power machine building, in manufacture of heat-exchange equipment and marine engineering. Excellent compatibility of titanium with biological tissues determines its application in development of implants.

Ukraine is one of the five countries of the world, which has a complete cycle of titanium production from extraction of titanium-containing ores, their dressing and production of spongy titanium to melting of titanium alloy ingots and production of virtual-



At the stand of PWI publishing house

ly complete spectrum of titanium semi-products , i.e. castings, forged pieces, bars, pipes and wires.

The basic of titanium conversion in Ukraine is technology of electron beam melting with intermediate crucible, which differs by a series of advantages in comparison with traditional method of ingot production by vacuum-arc remelting:

- complete elimination of consumable electrode pressing from a technological cycle, which requires special pressing equipment of large capacity;
- possibility of production of ingots of not only round section, but ingot-slabs of rectangular section used as billets for sheet products manufacture;
- guaranteed removal of refractory nonmetallic inclusions in the intermediate crucible and increase due to this of ingot metal quality;
- production of structurally and chemically homogeneous ingots with equiaxial structure;



Participants of the Conference at the entry to PWI main building

- increase of metal yield due to reduction of amount of remelts (one instead of two-three).

Developed at the E.O. Paton Electric Welding Institute of the NAS of Ukraine technological processes of electron beam melting provides the possibility to receive high-quality ingots of titanium and its alloys with homogeneous defect-free structure. Developed technologies allow reducing prime cost of titanium semi-finished products due to application of cheaper raw material and increase of through metal yield, and, respectively, rising competitiveness and expanding the fields of titanium application in different branches of industry.

Presentation on «EBW of thin-wall corrugated bearing airframes of titanium alloy and evaluation of their fatigue resistance» was made by K.S. Khripko (E.O. Paton Electric Welding Institute of the NAS of Ukraine, Kyiv). It shows economic advantages of EBW application and its technological peculiarities in production of beam structures.

S.P. Panov in his presentation «Titanium smelting in the laboratory disk bottom casting furnace» (Astron Ltd., New Zealand) provided the experimental investigations on development of new technology of production of titanium products or mastering of new compositions of titanium alloys in the furnace with bottom removal of the product of up to 100 kg mass. The tablets of titanium sponge are melted in the furnace using induction heating.

A.V. Ovchinnikov (Zaporozh'ye National Technical University of Ukraine) in presentation «Application of titanium in additive technologies» told about the main methods of product formation by additive technologies method. In his opinion it is possible to organize in Zaporozh'ye region a scientific-production cluster of additive technologies due to presence of production base for raw materials (ZTMC, ZMOZ) as well as research organizations.

Presentation on «Titanium and additive manufacture» was presented by D.V. Kovalchuk (PJSC «SPA Chervona Hvil'ya», Kyiv). It provided analysis of existing technologies of additive manufacture of titanium alloys, corresponding technical, technological and economical problems, was of their solution.

The presentations on the following topics were also made:

- «Conceptual solutions of production cycle in manufacture of parts from titanium alloys using additive technologies» (Yanko T.B., Dotsenko R.B., PJSC «Titanium Institute», PE «ELECTROMASH», Zaporozh'ye);

- «High Speed Friction Welding of Titanium Alloys — Structure and Properties of Joints» (Damian Miara<sup>1</sup>, Jolanta Matusiak<sup>1</sup>, Adam Pietras<sup>1</sup>, Maciej Krystian<sup>2</sup> (<sup>1</sup>Institut Spawalnictwa, Gliwice, Poland, <sup>2</sup>Austrian Institute of Technology, Vienna, Austria);

- «Effect of structure-phase state of titanium alloys on their mechanical properties depending on method and testing speed» (Markovsky P.E., G.V. Kurdyumov Institute for Metal Physics of the NAS of Ukraine, Kyiv);

- «Complexly-doped alloys based on titanium aluminides  $\gamma$ TiAl/ $\alpha_2$ Ti<sub>3</sub>Al» (Firstov S.A.<sup>1</sup>, Gornaya I.D.<sup>1</sup>, Podrezov Yu.N.<sup>1</sup>, Bondar A.A.<sup>1</sup>, Romanenko P.M.<sup>1</sup>, Goltvyanitsa V.S.<sup>2</sup>, Sheremetiev A.V.<sup>3</sup>, <sup>1</sup>I.M. Frantsevich Institute of Problems of Material Science of the NAS of Ukraine, Kyiv, <sup>2</sup>«Rial» LLC, <sup>3</sup>SE Ivchenko-Progress, Zaporozh'ye);

- «Theoretical description of equilibrium diagrams and phase transformations in titanium alloys of titanium-aluminum system» (Kostin V.A., Grigorenko G.M., Grigorenko S.G., E.O. Paton Electric Welding Institute of the NAS of Ukraine, Kyiv);

- «Peculiarities of production of strip cast billets of VT-1 grade or GRADE 2 of ungraded spongy titanium» (Kalinyuk A.N., Derecha A.Ya., Telin V.V., Kostenko V.I., Ivanov N.M. («Strategiya BM» LLC, Kyiv);

- «Microstructure and properties of multilayer materials based on Ti-6Al-4V alloy produced by powder technology» (Ivasishin O.M.<sup>1</sup>, Markovsky P.E.<sup>1</sup>, Savvakina D.G.<sup>1</sup>, Stachyuk A.A.<sup>1</sup>, Prikhodko S.V.<sup>2</sup>, <sup>1</sup>G.V. Kurdyumov Institute for Metal Physics of the NAS of Ukraine, Kyiv, <sup>2</sup>Material Science and Engineering department, University of California, Los-Angeles, USA).

45 poster papers were also presented at the Conference. They could be examined before and after the end of plenary papers of the Conference and during the breaks.

Exhibition «Production and welding of titanium» was held during the Conference in scope of PWI exposition. Zaporozh'ye Titanium and Magnesium Combine, PJSC «SPA Chervona Hvil'ya», SE STC «Paton-Armeniya» of E.O. Paton Electric Welding Institute of the NASU, «Vitova» LLC, «Melitek-Ukraine» LLC, «Spektro-Ukraine» LLC participated in it. A unique exposition of art objects from titanium presented by welder-artist Dmitrii Kushniruk was very interesting to Conference participants.

Participants of the Conference have a possibility to familiarize with PWI publishing activity, including

«Avtomaticeskaya Svarka» Journal, «Technical Diagnostics and Non-Destructive Testing», «The Paton Welding Journal» as well as books and collections of papers on welding and titanium production. The fourth issue of «Titanium. Technologies. Equipment» collection of papers (Kyiv: International Association «Welding», 2017, 254 p.) attracted particular interest. The collection includes more than 40 papers published mainly in «Sovremennaya Elektrometallurgiya» (Electrometallurgy Today) Journal and «Paton Welding Journal» for the period of 2014–2016 on electrometallurgy and welding of titanium and its alloys (previous three collections of papers «Titanium. Technologies. Equipment. Production», including the papers from «Sovremennaya Elektrometallurgiya» (Electrometallurgy Today) Journal and «Paton Welding Journal» for 2001–2004, 2005–2010, 2011–2013 are in open access on [www.patonpublishinghouse.com/rus/compilations](http://www.patonpublishinghouse.com/rus/compilations)).

At the end of the plenary paper session the participants of the Conference were invited to a boat trip over the Dnieper River. Discussions and arguments about a new topic of the Conference: Titanium — Metal of Present and Future, took place during the trip. In such informal environment it was possible to put questions to the academicians, directors of the institutes and enterprises, and, that is more important, get answers on them.

On June 13, the participants of the Conference had a tour to SE SPC «Titan» of E.O. Paton Electric Welding Institute. The enterprise is specialized on production of ingots of titanium and its alloys as well as heat-resistant alloys using electron beam remelting. Technology of surface flashing of produced EBM ingots, which replaces further machining of the ingots, was of high interest.

Proceedings of the Conference «Titanium 2018. Production and Application in Ukraine» will be published to the end of September 2018. They can be ordered in editorial board of «The Paton Welding Journal» or get in open access on <http://patonpublishinghouse.com/eng/proceedings> site.

Friendly, hospitable, creative atmosphere of the Conference promoted development of useful discussions, establishing business contacts. The participants of the Conference expressed unanimous approval of the proposal to carry out the Conference on titanium production and application on a constant basis.

The Organizing Committee expresses thanks and gratitude to PJSC «Titanium Institute», PJSC «SPA Chervona Hvilya», SE SPC «Titan» of E.O. Paton Electric Welding Institute and Center of Electron Beam Welding of E.O. Paton Electric Welding Institute for charity support of the Conference «Titanium 2018. Production and Application in Ukraine».

Prof. V.N. Lipodaev